




A Mathematical Description of Bacterial Chemotaxis in Response to Two Stimuli

Jeungeun Park¹ · Zahra Aminzare² 

Received: 26 May 2021 / Accepted: 26 October 2021 / Published online: 27 November 2021
© The Author(s), under exclusive licence to Society for Mathematical Biology 2021

Abstract

Bacteria are often exposed to multiple stimuli in complex environments, and their efficient chemotactic decisions are critical to survive and grow in their native environments. Bacterial responses to the environmental stimuli depend on the ratio of their corresponding chemoreceptors. By incorporating the signaling machinery of individual cells, we analyze the collective motion of a population of *Escherichia coli* bacteria in response to two stimuli, mainly serine and methyl-aspartate (MeAsp), in a one-dimensional and a two-dimensional environment, which is inspired by experimental results in Y. Kalinin *et al.*, J. Bacteriol. 192(7):1796–1800, 2010. Under suitable conditions, we show that if the ratio of the main chemoreceptors of individual cells, namely Tar/Tsr, is less than a specific threshold, the bacteria move to the gradient of serine, and if the ratio is greater than the threshold, the group of bacteria moves toward the gradient of MeAsp. Finally, we examine the theory with Monte Carlo agent-based simulations and verify that our results qualitatively agree well with the experimental results in Y. Kalinin *et al.* (2010).

Keywords Chemotaxis · Multi-scale dynamics · Population dynamics · Intracellular decision making · Fokker–Planck equations · Advection–diffusion equations · Monte Carlo simulations

1 Introduction

The preferred movement of a bacterium along the gradient of chemical substances, the so-called chemotaxis, includes a directed movement (run) and a relatively short random

✉ Zahra Aminzare
zahra-aminzare@uiowa.edu

Jeungeun Park
parkj21@newpaltz.edu

¹ Department of Mathematics, State University of New York at New Paltz, New York, NY, USA

² Department of Mathematics, University of Iowa, Iowa City, IA, USA

turning (tumble). See, e.g., Berg and Brown (1972), Macnab and Koshland (1972) for *Escherichia coli* (*E. coli*) and *Salmonella typhimurium* chemotaxis. Each bacterium carries an internal state which may be modeled by a system of ordinary differential equations. In the presence of a stimulus in the environment, each cell changes its direction at random, with a tumbling rate which depends on the internal state, biasing moves toward more favorable environments or away from noxious substances.

In natural environments, bacteria are often exposed to multiple chemical stimuli. To navigate toward a favorable environment, they choose their directions of movement based on environmental perception, individual preferences, and interaction with others. Also, each individual's decision characterizes the behavior of a group of bacteria. Thus, understanding how bacterium chooses between multiple stimuli is essential to study bacterial chemotaxis at the population level.

In the case of *E. coli*, chemical signals are often detected via five main chemoreceptors, namely Tar, Tsr, Tap, Trg, and Aer Vladimirov and Sourjik (2009). In Kalinin et al. (2010), where responses of *E. coli* to two chemoattractant signals are demonstrated, it is shown that the expression levels of the most abundant receptors, Tar and Tsr, are determined by the bacterial density in a batch-mode culture within the growth phase; in turn, the ratio of these receptors differentiates their chemical preferences.

Inspired by the experimental results of Kalinin et al. (2010), our goal of this work is to incorporate the bacterial decision-making process into a mathematical model and investigate the corresponding collective behavior observed in Kalinin et al. (2010). To this end, we consider a population of bacteria in a one-dimensional and a two-dimensional spatial domain occupied by two stimuli that their temporal rates are assumed to be zero. First, we employ a Fokker–Planck-type master equation (also known as balance equation Alt (1980)) to describe the bacterial chemotaxis. This (microscopic) model enables us to incorporate the internal dynamics of *E. coli* representing the chemotaxis signaling pathway (Tu et al. 2008; Edgington and Tindall 2018). Then, we describe the *E. coli* population dynamics by a (macroscopic) advection–diffusion equation, which is analogous to the classic Keller–Segel model (Keller and Segel 1971), and can be derived from the microscopic model by the tools developed in Erban and Othmer (2004).

Mathematical modeling aiming to understand the behavior of bacteria population in response to external signals has been extensively studied (see Tindall et al. (2008) for a review on multi-scaling model approaches for chemotaxis). These studies have been discussed along with detailed mathematical models for the entire signal transduction network, first modeled by Barkai and Leibler (1997) and Spiro et al. (1997). In Erban and Othmer (2004, 2005), the authors studied *E. coli* chemotaxis in response to a single stimulus in a one-dimensional and an arbitrary dimensional space, respectively. These studies were generalized in Xue and Othmer (2009) to multiple space- and time-dependent signals by applying a general type of receptor-based response laws (Othmer and Stevens 1997; Painter et al. 2000). These works considered a *toy* model for the internal dynamics. In Aminzare and Sontag (2013), Menolascina et al. (2017), the authors allow arbitrary one-dimensional internal dynamics in response to a time-independent signal and more realistic models for *E. coli* internal dynamics given in Tu et al. (2008), Kalinin et al. (2009). The theory was further generalized to higher-dimensional space and multiple signals in Xue (2015), Xue and Yang (2016).

The authors in Hu and Tu (2014) incorporated *E. coli* signaling pathway from Tu et al. (2008) into a one-dimensional macroscopic equation in order to understand various taxis behaviors in Salman and Libchaber (2007), Demir et al. (2011), Yang and Sourjik (2012). The macroscopic model was also validated by comparing with available experimental data that show the ratio of Tar and Tsr affects bacterial thermotaxis and pH taxis.

Our contributions toward understanding the dynamics of a population of bacteria in response to two stimuli are as follows. First, we incorporate a relatively *general* class of one-dimensional internal dynamics into a one- and a two-dimensional microscopic equation from which one can derive a macroscopic equation. Second, we use the macroscopic model for a population of *E. coli* with a mechanistically realistic, while a mathematically tractable, model of internal dynamics and analyze the response of *E. coli* to two stimuli in a one- and a two-dimensional environment. By analyzing the steady-state solution of the macroscopic equation, we further show that there is a critical ratio of receptors that determines bacterial movement toward their favored chemical. Finally, we demonstrate some Monte Carlo agent-based simulations for different types of stimuli and compare them with numerical solutions of the model. We also explain that the Monte Carlo simulations results agree well with the experimental results of Kalinin et al. (2010).

The remainder of the paper is organized as follows. In Sect. 2, we first review the internal dynamics of *E. coli* which describe how the cells can produce runs and tumbles. Then, given a general internal dynamics of bacteria, we introduce a (forward) Fokker–Planck equation which describes the dynamics of a probability distribution of a population of bacteria. By applying specific *E. coli* internal dynamics, the stochastic equation is approximated by a one-dimensional (respectively, two-dimensional) advection–diffusion equation in Sect. 3 (respectively, Section 4). Also, a bifurcation parameter and its value of bacterial chemical preferences are identified. This result is also verified when comparing the solutions to the advection–diffusion equation with Monte Carlo agent-based simulation and verified by comparing the solutions with Monte Carlo agent-based simulations. In Sect. 5, we conclude with a brief summary and discussion of future directions. All the parameters are given in Table 1 and Table 2 in an Appendix.

2 Microscopic Behavior of a Population of *E. coli* Bacteria

We briefly review the internal dynamics of *E. coli* which transfer a signal of the environment into a motor rotation for a run or a tumble (see Tu et al. (2008), Kalinin et al. (2009), Jiang et al. (2010) for more details). Then, following Erban and Othmer (2004), Aminzare and Sontag (2013), Othmer et al. (1988), we derive a probabilistic equation which describes *microscopic* dynamics of a population of bacteria with a given internal dynamics. Later, in the following section, we use the microscopic equation to derive a *macroscopic* equation which approximates the dynamics of a population of bacteria by integrating the internal dynamics of all the bacteria.

2.1 The Internal Dynamics of *E. coli*: A Brief Review

E. coli bacteria use four to six helical flagella that are connected to rotary motors in their cell wall to swim. Their swimming patterns are characterized as a random walk, consisting of long runs (~ 1 sec) and short tumbles (~ 0.1 sec). When a cell senses an increasing of external attractant gradient, the run length is extended (Berg and Brown 1972; Berg and Turner 1990). The receptors in the membrane of the cells, which receive the signals, and the flagellar motors, which produce runs and tumbles, are connected by a signaling pathway within the cell, as shown in Figure 1(left), Wadhams and Armitage (2004). The receptors form hetero-trimers of homo-dimers, which is basic signaling units, and the clusters of mixed trimers of dimers link to a histidine kinase CheA through a linker protein CheW (Endres et al. 2008; Hansen et al. 2010; Xin and Othmer 2012; Lai et al. 2017). We note that individual receptors cannot activate CheA, and hence, in this paper, we refer to the dimers as receptors.

In the absence of an attractant gradient, CheA autophosphorylates and produces CheA-P. The phosphoryl group of CheA-P transfers to either CheY or CheB. Phosphorylated CheY (denoted by CheY-P) enhances the probability of switching to a clockwise motor rotation by binding to a protein FilM, a component for switching the direction of motor rotation (Welch et al. 1993; Bren et al. 1996; Lipkow et al. 2005), and thus the tumbling rate increases. The clockwise motor rotation is quickly modulated as CheZ accelerates the dephosphorylation of CheY-P in Lipkow (2006).

In the presence of an attractant gradient, a ligand binds to a receptor and inhibits the activity of CheA, followed by decreasing the CheY-P and CheB-P levels. The reduction in CheY-P levels lengthens the run with a counter-clockwise motor rotation.

To respond to further changes in the concentration of a gradient, CheR and CheB-P mediate adaptation. On the one hand, CheR methylates the receptors and hence enhances CheA activity (Springer and Koshland 1977). On the other hand, CheB-P demethylates the receptors and consequently inhibits the activity of CheA (Stock and Koshland 1978). Therefore, when an attractant gradient is sensed, the CheA-P level, and thus the CheB-P level decrease. While the CheB-P level decreases, the receptors are methylated by CheR, and they return to their pre-stimulus state, followed by the pre-stimulus values of CheA activity, CheA-P and CheY-P levels, and motor bias. This process is called an adaptation of methylation.

The intracellular chemotaxis signaling pathway, which contains three main phosphorylation groups and the receptor methylation level, can be mathematically modeled by four coupled ordinary differential equations (ODEs) that consist of three biochemical equations for CheA-P, CheB-P, and CheY-P, and one equation for the methylation level of receptors. However, the phosphorylation processes and the methylation process occur at different time scales, and one can reduce the four-dimensional system into a three-, two-, or even a one-dimensional system. In Edgington and Tindall (2018), the authors explained these reductions in detail.

It is known that the adaptation process of methylation is much slower than the other dynamics in the signaling pathway (Erban and Othmer 2005; Bray and Bourret 1995; Terwilliger et al. 1986; Simms et al. 1987). Therefore, assuming quasi-equilibrium approximations for CheA-P, CheB-P, and CheY-P, we consider a one-dimensional

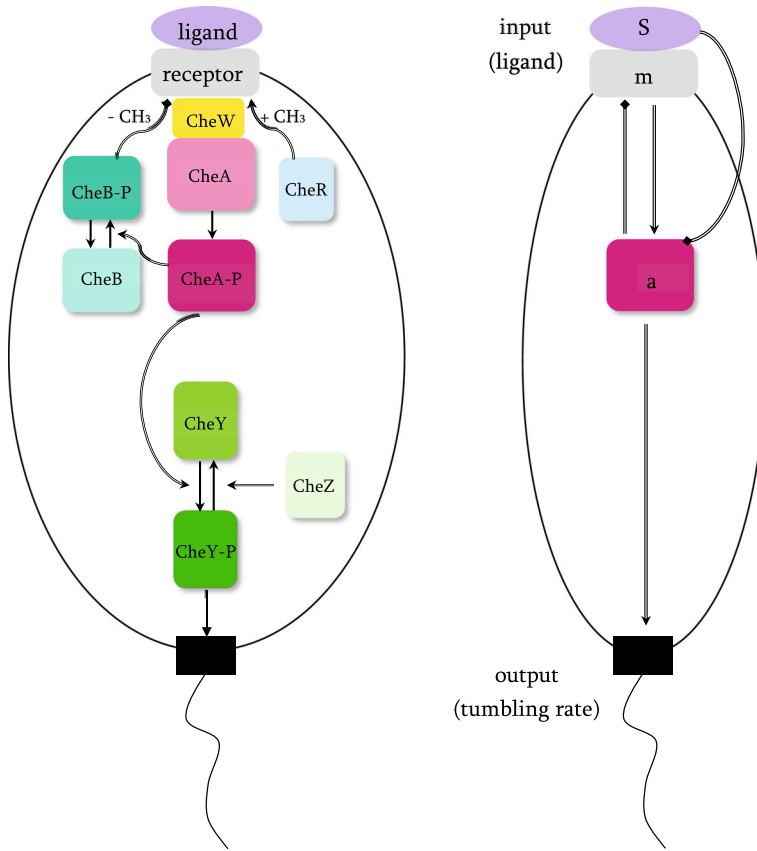


Fig. 1 Left: *E. coli* signaling pathway. Binding ligands to receptors, the signal is transduced to the flagellar motor via six cytoplasmic chemotaxis proteins. Right: An input–output representation of *E. coli* signaling pathway. The internal signaling pathway shown in left is reduced to the interaction between the methylation level m and the kinase activity a . This interaction, which depends on ligand concentration S (input), controls the motor rotation by changing the tumbling rate (output). See Sect. 2.1 for detailed description

reduction model for the methylation level of receptors, as developed in Tu et al. (2008).

Consider the following input–output dynamics for the chemotaxis signaling pathway, as shown in Figure 1(right). The ligand concentration, denoted by S , and the tumbling rate, denoted by λ , represent the input and the output, respectively. As explained above, binding the ligand to the receptor inhibits the activity of CheA, denoted by a . On the other hand, the methyl group (denoted by m) in the receptors enhances the activity of a . Therefore, $a = G(S, m)$ can be described as an increasing function of m and a decreasing function of S .

As described earlier, the kinase activity of CheA enhances the CheB-P level, and CheB-P reduces the methylation level of the receptors. Consequently, the kinase activity a reduces the methylation level m , indirectly. So, the dynamics of m can be described by $dm/dt = F(a)$, where F is a decreasing function of a .

Several models for methylation dynamics (F) and kinase activity function (G) have been developed. See, e.g., Tu et al. (2008), Edgington and Tindall (2018), Vladimirov et al. (2008), Clausznitzer et al. (2010). For ease of calculation, we choose models for F and G as described in (1) and (2). Despite of the simplicity, the models capture the essential features such as receptor cooperativity, methylation on kinase activity, and adaptation for *E. coli* signaling pathway, and they were verified by existing experiments. More details are discussed below.

Note that the tumbling rate λ is controlled by the level of CheY-P, which is affected by the kinase activity. Therefore, λ can be modeled by an increasing function of a , as described in (5).

Following the experimental setup in Kalinin et al. (2010), we consider two stimuli: S_1 and S_2 , which, respectively, stand for methyl-aspartate (MeAsp) and serine, and can be sensed by Tar and Tsr, which are the most abundant chemoreceptors in the *E. coli* chemotaxis network. Furthermore, since the experiments in Kalinin et al. (2010) are designed to keep the external signals S_1 and S_2 constant in time, we assume that S_1 and S_2 only depend on the spatial variable \mathbf{x} and are independent of time t : $S_1 = S_1(\mathbf{x})$ and $S_2 = S_2(\mathbf{x})$.

Remark 1 In a mixed cluster of receptors, not only adaptation occurs locally and is ligand specific, but also interactions among receptors are crucial to signal amplification and integration. Models for a mixed-receptor cluster with crosstalk among different types of receptors have been developed to understand how a mixed-receptor cluster differentiates ligand types and adapts to the individual stimuli (e.g., Hansen et al. (2010), Xin and Othmer (2012), Lai et al. (2017), Endres and Wingreen (2006), Lan et al. (2011) and reference therein). In this work, however, we do not attempt to capture all the details on receptor crosstalk, and consequently methylation crosstalk and ligand-specific adaptation are not considered. Instead, we are interested in the *total* receptor kinase activity of the whole receptor cluster, and use the *average* methylation level of the entire receptor rather than the methylation dynamics for different types of receptors separately, as in Hu and Tu (2014). Due to the simplicity of our model, it is unable to describe processes that depend on activities of individual receptors in the cluster; however, it makes our model analytically solvable, and still captures the essential features such as receptor cooperativity, effects of methylation on kinase activity, and adaptation.

Following Hu and Tu (2014); Mello and Tu (2005), Neumann et al. (2010), we let a heterogeneous Monod–Wyman–Changeux (MWC) model (Monod et al. 1965) describe the *total* kinase activity a :

$$G(S_1, S_2, m) = \frac{1}{1 + \eta_0(m)\eta_1(S_1)\eta_2(S_2)}, \quad (1)$$

where $\eta_0(m)\eta_1(S_1)\eta_2(S_2)$ is derived from the total free energy difference between the active and inactive states. According to Tu et al. (2008), Jiang et al. (2010), Sourjik and Berg (2002), Shimizu et al. (2006), Mello and Tu (2007), the methylation-dependent

free energy gives

$$\eta_0(m) = \exp(N\alpha(m_0 - m)),$$

where N is the number of the responding receptors in the cluster, and α and m_0 denote the free-energy per added methylation group and a reference methylation level, respectively. The ligand-dependent free-energy obtains

$$\eta_i(S_i) = \left(\frac{1 + S_i/K_I^i}{1 + S_i/K_A^i} \right)^{Nr_i},$$

where K_I^i and K_A^i are the dissociation constants of the corresponding ligand ($i = 1$ for MeAsp, $i = 2$ for serine) to the inactive and the active receptor ($i = 1$ for Tar, $i = 2$ for Tsr). The constant parameters r_1 and r_2 are the fraction of receptors Tar and Tsr in the receptor cluster, respectively. We assume that $r_1 + r_2 = 1$ and r_1N and r_2N are the number of the receptors binding to the corresponding ligand.

The average methylation level of receptors, m , evolves slowly, and can be described by the following equation (Tu et al. 2008; Jiang et al. 2010):

$$\frac{dm}{dt} = F(a) = \frac{a_0 - a}{\tau_a}, \tag{2}$$

where $\tau_a \gg 1$ is the time scale and a_0 is a constant which represents the adaptation level of a , i.e., when $a > a_0$, $dm/dt < 0$ and hence m and consequently a decrease. When $a < a_0$, $dm/dt > 0$ and hence m and consequently a increase.

In what follows, we denote a state variable by a in (1) that depends on m which restores a to the adapted level a_0 . Taking time derivative of a gives:

$$\frac{da}{dt} = \frac{\partial a}{\partial m} \frac{dm}{dt} + \frac{\partial a}{\partial S_1} \nabla_{\mathbf{x}} S_1 \cdot \frac{d\mathbf{x}}{dt} + \frac{\partial a}{\partial S_2} \nabla_{\mathbf{x}} S_2 \cdot \frac{d\mathbf{x}}{dt}. \tag{3}$$

Using (1) for $a = G(S, m)$, we obtain

$$\frac{\partial a}{\partial m} = \alpha Na(1 - a), \quad \frac{\partial a}{\partial S_i} = Na(a - 1)r_i \frac{1/K_I^i - 1/K_A^i}{(1 + S_i/K_I^i)(1 + S_i/K_A^i)}.$$

For $i = 1, 2$, we assume that for any \mathbf{x} ,

$$K_I^i \ll S_i(\mathbf{x}) \ll K_A^i,$$

as in Tu et al. (2008), Jiang et al. (2010). This assumption guarantees scale-invariant behavior of *E. coli* in response to external signals, which was mathematically predicted in Shoval et al. (2010) and experimentally verified in Lazova et al. (2011). Scale-invariance property of a system means that the system does not distinguish between an input (here, S_1 or S_2) and its scaled version (e.g., $p_1 S_1$ or $p_2 S_2$). For more details,

see Edgington and Tindall (2018) and Shoval et al. (2011). Using this assumption, we make the following approximation

$$\frac{1/K_I^i - 1/K_A^i}{(1 + S_i/K_I^i)(1 + S_i/K_A^i)} \approx \frac{1}{S_i}.$$

Therefore,

$$\frac{da}{dt} = \alpha Na(1 - a) \frac{a_0 - a}{\tau_a} + Na(a - 1) \left(r_1 \frac{\nabla_{\mathbf{x}} S_1 \cdot d\mathbf{x}/dt}{S_1} + r_2 \frac{\nabla_{\mathbf{x}} S_2 \cdot d\mathbf{x}/dt}{S_2} \right). \tag{4}$$

Experimental data on the parameters used in this section are listed in Table 1.

Remark 2 *E. coli* bacteria can also sense pH changes, and their internal dynamics during pH taxis is analogous to that during chemotaxis. For example, according to Hu and Tu (2014), Demir et al. (2011), Yang and Sourjik (2012), Tar receptors are attracted to a decrease in pH, but Tsr receptors show the opposite response. Taking into account two chemical stimuli with different pH levels, we can apply the heterogeneous MWC model and use the following assumptions to derive the internal dynamics for pH:

$$K_I^1 \ll S_1(\mathbf{x}) \ll K_A^1, \quad \text{and} \quad K_A^2 \ll S_2(\mathbf{x}) \ll K_I^2,$$

which yield

$$\frac{1/K_I^1 - 1/K_A^1}{(1 + S_1/K_I^1)(1 + S_1/K_A^1)} \approx \frac{1}{S_1}, \quad \text{and} \quad \frac{1/K_I^2 - 1/K_A^2}{(1 + S_2/K_I^2)(1 + S_2/K_A^2)} \approx \frac{-1}{S_2}.$$

As a result of the slow adaptation process (2), bacteria use their methylation state as a short-term memory store to compare changes of stimuli temporarily during a run. This process helps the bacteria to run or tumble effectively toward their preferred location. According to experimental observations and measurements, the tumbling rate function can be described as

$$\lambda(a) = \lambda_0 + \frac{1}{\tau} \left(\frac{a}{a_0} \right)^H, \tag{5}$$

where λ_0 , H , and τ denote the rotational diffusion, the Hill coefficient of flagellar motor’s response curve, and the average run time, respectively, and a_0 is as given in (2). Note that since a depends on S , we may write $\lambda = \lambda(a, S)$ (see Sect. 2.2). More details about the physical meaning of these parameters can be found in Hu and Tu (2014), Jiang et al. (2010), Sourjik and Berg (2002). The parameter values are shown in Table 1.

2.2 A Fokker–Planck Equation Describing a Population of Bacteria

In what follows, we describe the motion of a population of bacteria by incorporating their internal dynamics.

Let $p(\mathbf{x}, \mathbf{a}, \mathbf{v}, t)$ be a probability density function describing a population of bacteria, modeled in a $2\mathcal{N} + \mathcal{M} + 1$ -dimensional phase space, where time $t \in \mathbb{R}$, $\mathbf{x} = (x_1, \dots, x_{\mathcal{N}}) \in \mathbb{R}^{\mathcal{N}}$ (we will specialize to $\mathcal{N} = 1, 2$) denotes the position of a cell centroid, $\mathbf{a} = (a_1, \dots, a_{\mathcal{M}}) \in A \subset \mathbb{R}^{\mathcal{M}}$ (we will specialize to $\mathcal{M} = 1$) denotes the internal dynamics of the cell, and $\mathbf{v} = (v_1, \dots, v_{\mathcal{N}}) \in V \subset \mathbb{R}^{\mathcal{N}}$ denotes its velocity, $d\mathbf{x}/dt = \mathbf{v}$. The vector $\mathbf{S}(\mathbf{x}, t) = (S_1(\mathbf{x}, t), \dots, S_{\mathcal{K}}(\mathbf{x}, t)) \in \mathbb{R}^{\mathcal{K}}$ represents the concentration of extracellular signals in the environment (we will assume that \mathbf{S} only depends on \mathbf{x} as in Sect. 2.1 and Kalinin et al. (2010)).

Let the following system of ODEs describe the evolution of the intracellular state, in the presence of the extracellular signal \mathbf{S} :

$$\frac{d\mathbf{a}}{dt} = f(\mathbf{a}, \mathbf{S}), \tag{6}$$

where $f: \mathbb{R}^{\mathcal{M}} \times \mathbb{R}^{\mathcal{K}} \rightarrow \mathbb{R}^{\mathcal{M}}$ is a continuously differentiable function with respect to each component, i.e., $f \in C^1(\mathbb{R}^{\mathcal{M}} \times \mathbb{R}^{\mathcal{K}})$.

Assuming constant velocity, $dv_i/dt = 0$, the evolution of $p = p(\mathbf{x}, \mathbf{a}, \mathbf{v}, t)$ with turning rate $\lambda = \lambda(\mathbf{a}, \mathbf{S})$ is governed by the following forward Fokker–Planck equation describing a velocity-jump process (Alt 1980; Othmer et al. 1988):

$$\frac{\partial p}{\partial t} + \nabla_{\mathbf{x}} \cdot \mathbf{v}p + \nabla_{\mathbf{a}} \cdot f p = -\lambda(\mathbf{a}, \mathbf{S})p + \int_V \lambda(\mathbf{a}, \mathbf{S})T(\mathbf{a}, \mathbf{v}, \mathbf{v}')p(\mathbf{x}, \mathbf{a}, \mathbf{v}', t) d\mathbf{v}', \tag{7}$$

where the non-negative kernel $T(\mathbf{a}, \mathbf{v}, \mathbf{v}')$ is the probability that the bacteria change the velocity from \mathbf{v}' to \mathbf{v} , and

$$\int_V T(\mathbf{a}, \mathbf{v}, \mathbf{v}') d\mathbf{v}' = 1.$$

Equation (7) is not tractable mathematically and is hard to be validated by typical experimental techniques. The goal is to use the *microscopic* model (7), and derive a *macroscopic* model for chemotaxis in a one-dimensional space (in Sect. 3) and a two-dimensional space (in Sect. 4), i.e., an equation for the marginal density

$$n(\mathbf{x}, t) = \int_V \int_A p(\mathbf{x}, \mathbf{a}, \mathbf{v}, t) d\mathbf{a} d\mathbf{v},$$

with $\mathcal{N} = 1$ or 2 , $\mathcal{M} = 1$, and $\mathcal{K} = 2$; $n(\mathbf{x}, t)$ is the number of individuals which at time t are located at position \mathbf{x} , whatever their internal dynamics and velocity are.

Note that the theory works for any arbitrary \mathcal{K} . However, we are interested in two extracellular signals, so we only consider $\mathcal{K} = 2$.

3 *E. coli* Preferences in Response to Two Stimuli in a One-Dimensional Space

In this section, we study the behavior of bacteria in response to two stimuli in a one-dimensional space. First, we derive the corresponding macroscopic equation; then analyze its steady-state behavior and discuss bacteria preferences. Then, we compare the numerical solutions of the model and Monte Carlo simulations and discuss how they agree with experimental results.

3.1 Advection–Diffusion Equations and Integration of the Biochemistry of *E. coli* Chemotaxis

First, we assume that the bacteria move in a one-dimensional space, i.e., a finite interval $[0, L]$ where we assume L is sufficiently large. We let $p^\pm(x, a, t) = p(x, a, \pm v, t)$ denote the density of the bacteria, located at $x \in [0, L]$, moving to the right and left, respectively, and let $f^\pm = f_0 \pm v f_1$ describe their corresponding internal state. Here, $v > 0$ represents the speed of the bacteria, and we assume that v is constant. Then, the Fokker–Planck equation (7) becomes

$$\frac{\partial p^+}{\partial t} + v \frac{\partial p^+}{\partial x} + \frac{\partial}{\partial a} [f^+(a, S) p^+] = \frac{1}{2} \lambda(a, S)(p^- - p^+), \tag{8}$$

$$\frac{\partial p^-}{\partial t} - v \frac{\partial p^-}{\partial x} + \frac{\partial}{\partial a} [f^-(a, S) p^-] = \frac{1}{2} \lambda(a, S)(p^+ - p^-). \tag{9}$$

Following Erban and Othmer (2004), Erban and Othmer (2005), Xue and Othmer (2009), Aminzare and Sontag (2013), Xue (2015), under a decay condition for p^\pm , some conditions on the internal dynamics (for example, shallow conditions for the stimuli—see Proposition 1), moment closure techniques, and parabolic scaling, a general advection–diffusion equation for the marginal density

$$n(x, t) = \int_A (p^+(x, a, t) + p^-(x, a, t)) da$$

can be derived from Equations (8)-(9) as follows

$$\frac{\partial n}{\partial t} = \frac{\partial}{\partial x} \left(\frac{v^2}{\alpha_0} \frac{\partial n}{\partial x} - \frac{\alpha_1 B_0 v^2}{\alpha_0(A_1 - \alpha_0)} n \right). \tag{10}$$

Here, α_i , A_i , and B_i are the Taylor constants of λ , f_0 , and f_1 , respectively:

$$\begin{aligned} \lambda &= \alpha_0 + \alpha_1 a + \dots, \\ f_0 &= A_0 + A_1 a + \dots, \\ f_1 &= B_0 + B_1 a + \dots. \end{aligned}$$

All the Taylor constants depend on $S = S(x)$.

In what follows, we determine the terms in the advection–diffusion equation (10) for a population of *E. coli* bacteria in a spatial domain $[0, L]$ equipped with two chemical gradients MeAsp, denoted by $S_1(x)$, and serine, denoted by $S_2(x)$. We further assume that S_1 and S_2 are, respectively, increasing and decreasing functions on $[0, L]$, i.e., MeAsp accumulates near $x = L$ and serine accumulates near $x = 0$. As we discussed in Sect. 2.1, in a one-dimensional space, the internal state of *E. coli* evolves according to Equation (4). Following Aminzare and Sontag (2013), Xue (2015), we state the following proposition, in which all the parameters and functions are as described in Sect. 2.1.

Proposition 1 *Assume that the density functions p^\pm satisfy the decay condition*

$$p^\pm(x, a, t) \leq C(x, t)e^{-c(x,t)a}$$

for some functions $C, c : \mathbb{R} \times [0, \infty) \rightarrow \mathbb{R}_{>0}$. With the fraction of two receptors, r_1 and r_2 , suppose that the stimuli S_1 and S_2 satisfy the shallow condition

$$\left| r_1 \frac{S'_1(x)}{S_1(x)} + r_2 \frac{S'_2(x)}{S_2(x)} \right| \leq \min\{q, 1 - q\} \frac{p}{v}, \quad \forall x \in [0, L], \tag{11}$$

where $q = a_0$ and $p = \frac{\alpha}{\tau_a}$ represent the adapted value and the speed of adaptation, respectively. Then, for the given internal dynamics (4), the dynamics of a population of *E. coli*, $n(x, t)$, can be approximated by the advection–diffusion

$$\frac{\partial n}{\partial t} = \frac{\partial}{\partial x} \left(D \frac{\partial n}{\partial x} - \chi V(x)n \right), \tag{12}$$

where the diffusion coefficient D and the advection terms χ and $V(x)$ are as follows:

$$D = \frac{v^2}{\lambda_0 + rq^H}, \quad \chi = \frac{rNHq^H(q - 1)v^2}{(\lambda_0 + rq^H)(Npq(q - 1) - \lambda_0 - rq^H)}, \tag{13}$$

$$V(x) = r_1 \frac{S'_1(x)}{S_1(x)} + r_2 \frac{S'_2(x)}{S_2(x)}. \tag{14}$$

Note that the condition (11) holds if either the adaptation rate p is large or r_1, r_2, S_1 and S_2 are chosen so that the left hand side (LHS) of (11) is small, i.e., the shallow condition is equivalent to either small changes in the environment or fast adaptation. For the case where the whole receptor cluster contains both Tar and Tsr, we define

$$\gamma := \frac{r_1}{r_2}, \tag{15}$$

which is the ratio Tar/Tsr, to reduce the number of parameters. Recall that $r_1 + r_2 = 1$, so indeed $r_1 = \frac{\gamma}{1+\gamma}$ and $r_2 = \frac{1}{1+\gamma}$. As an example, a role of γ and the shallow condition will be discussed in Sect. 3.3 in more detail by choosing specific S_1 and S_2 of our interest.

Following the experimental setup of Kalinin et al. (2010) in which the population of the bacteria is conserved in time, we impose the following zero flux boundary conditions at $x = 0$ and $x = L$. For any $t \geq 0$,

$$\frac{\partial n}{\partial x}(0, t) = \frac{\chi}{D}V(0)n(0, t) \quad \text{and} \quad \frac{\partial n}{\partial x}(L, t) = \frac{\chi}{D}V(L)n(L, t). \tag{16}$$

3.2 Bifurcation of Bacterial Chemotactic Preference

The bacterial responses to MeAsp and serine depend on the ratio of their chemoreceptors Tar and Tsr, i.e., $\gamma = \text{Tar}/\text{Tsr}$, or equation (15). The goal is to find a positive γ^* and show that for $\gamma > \gamma^*$ the bacteria tend to move toward a gradient of increasing MeAsp (i.e., accumulate near $x = L$) and for $\gamma < \gamma^*$ they move toward a gradient of increasing serine (i.e., accumulate near $x = 0$). To determine such a γ^* , we look at a steady state of the advection–diffusion equation (12) with boundary condition (16). Under some assumptions on S_1, S_2 and γ that guarantee the existence of a non-trivial solution (we provided details in Park and Aminzare (2020)), when the initial condition $n(x, 0)$ is non-trivial, a unique non-trivial steady state $\Phi(x)$ of (12) exists as follows:

$$\Phi(x) = \Phi(c_0) \exp \left\{ \frac{\chi}{D} \int_{c_0}^x V(y)dy \right\} \tag{17}$$

for some c_0 such that $\Phi(c_0) > 0$. Indeed, there is such a c_0 by (16):

$$\begin{aligned} \frac{d}{dt} \int_0^L n(x, t)dx = 0 &\Rightarrow \int_0^L n(x, t)dx = \text{constant} > 0 \\ &\Rightarrow \lim_{t \rightarrow \infty} \int_0^L n(x, t)dx = \int_0^L \Phi(x)dx = \text{constant} > 0 \\ &\Rightarrow \text{there exists } c_0 \text{ such that } \Phi(c_0) > 0. \end{aligned}$$

Assuming that the bacteria start from a point $x_0 \in (0, L)$, they move toward a gradient of increasing MeAsp (respectively, serine) and accumulate near $x = L$ (respectively, $x = 0$), if the steady-state solution of the advection–diffusion equation (12) admits a maximum on the right (respectively, left) sub-interval $(x_0, L]$ (respectively, $[0, x_0)$). Therefore, in what follows, we find conditions that $\Phi(x)$ admits a maximum on the right sub-interval $(x_0, L]$ or the left sub-interval $[0, x_0)$.

In what follows, we write V as a function of both x and γ , $V = V(x, \gamma)$. Considering the fact that $\Phi'(x) = \frac{\chi}{D}V(x, \gamma)\Phi(x)$ and $\Phi(x) > 0$, Φ takes a unique maximum at $x^* \in [0, L]$ if, for any $\gamma > 0$, either V does not change sign or V is a non-increasing function of x and $V(x^*, \gamma) = 0$. Now we are ready to find γ^* in the following lemma.

Lemma 1 *Assume the bacteria start at $x_0 \in [0, L]$ and for any $\gamma > 0$, $\partial V/\partial x \leq 0$. Also, assume that S_1 and S_2 are, respectively, increasing and decreasing functions on $[0, L]$. Then, there exists $\gamma^* > 0$ such that $V(x_0, \gamma^*) = 0$ and for $\gamma > \gamma^*$ the bacteria accumulate on the right side of x_0 and for $\gamma < \gamma^*$ they accumulate on the left side.*

Proof A simple calculation shows that $V(x, \gamma) = 0$ if and only if

$$\gamma(x) = -\frac{S_2'(x)/S_2(x)}{S_1'(x)/S_1(x)}.$$

Let $\gamma^* := \gamma(x_0)$. For $\gamma > \gamma^*$, $V(x_0, \gamma) > 0$, therefore, since $\partial V/\partial x \leq 0$, Φ takes its maximum (either $x = L$ or $x = x^* < L$) on the right side of x_0 , and hence the bacteria accumulate toward the right side of x_0 . Similarly, if $\gamma < \gamma^*$, $V(x_0, \gamma) < 0$, and hence Φ takes its maximum (either $x = 0$ or $x = x^* > 0$) on the left side of x_0 , and hence the bacteria accumulate toward the left side of x_0 . \square

We refer to γ and γ^* as the bifurcation parameter and bifurcation value, respectively, since at $\gamma = \gamma^*$ the direction of the bacterial changes. See Figure 2.

Note that if the bacteria are initially distributed on $[0, L]$ instead of locating on a single point x_0 , we consider $\gamma^* = \gamma^*(L/2)$ as the bifurcation value.

In the following section, we consider two sets of stimuli: (i) S_1 linear and increasing, S_2 linear and decreasing; (ii) S_1 exponential and increasing, S_2 exponential and decreasing. We also assume that the bacteria are located at $x_0 = L/2$ initially. In both cases, $V(x, \gamma)$ is a decreasing function on $[0, L]$. Hence, the conditions of Lemma 1 hold and, therefore, γ^* can be determined based on the initial location of the bacteria, i.e., $x_0 = L/2$.

3.3 Monte Carlo Agent-based Simulations in a One-dimensional Space

To show that the advection–diffusion equation (12) with boundary condition (16) is a good approximation for the microscopic description of *E. coli* chemotaxis, we run a Monte Carlo agent-based simulation. A detailed description of the Monte Carlo simulation is given in Table 2.

The following computational setting of our Monte Carlo agent-based simulation is motivated by the experimental setup in Kalinin et al. (2010).

Spatial Domain. A one-dimensional channel of length of $400\mu m$ ($x \in [0, 400]$).

Stimuli. Along the two sides of the channel two opposing chemical signals, $S_1(x)$ and $S_2(x)$, flow and diffuse across the channel. Two opposing linear and two opposing exponential chemical signals are considered in Sects. 3.3.1 and 3.3.2, respectively.

Initial Condition. At $t = 0$ (sec), an ensemble of 100,000 agents is located in the center of the channel ($x = 200$).

Boundary Conditions. When a cell reaches a boundary, we relocate the cell to stay inside the domain, i.e., zero flux boundary condition is applied.

Simulation Duration. We simulate the bacterial behavior for 200 sec, $t \in [0, 200]$. It is observed that the solution of each simulation in this section becomes stationary at $t = 200$.

To illustrate distributions of the cells, we display histograms with 100 equal-sized bins.

We use an explicit finite difference method to numerically solve the advection–diffusion equation (12) with the boundary condition (16).

In the following examples, we compare the solutions of the macroscopic equation (12) with boundary conditions (16) with results of the Monte Carlo simulation. Further, for each case, we compute the bifurcation value γ^* defined in Sect. 3.2. To measure bacterial preference, we define the chemotactic migration coefficient (CMC):

$$CMC_x(t) = \frac{\text{mean}(x(t)) - 200}{200}. \tag{18}$$

In the Monte Carlo simulation, $\text{mean}(x(t))$ is the average of individual positions x_i at time t across the channel, i.e., $\text{mean}_i(x_i(t))$. For a solution $n(x, t)$ of (12), $\text{mean}(x(t))$ is the expectation value of the probability density $n(x, t)$, i.e., $\int_0^L xn(x, t)dx$. The absolute value of CMC_x determines the displacement of the bacteria in x -direction. The sign of CMC_x indicates their preference to the right or left. When $CMC_x > 0$ (respectively, $CMC_x < 0$), the bacteria tend to move to the right, i.e., above $x = 200$ (respectively, left, i.e., below $x = 200$).

3.3.1 Chemotaxis in Response to Two Linear Gradients

To demonstrate responses of *E. coli* to two opposing linear gradients MeAsp and serine, and following the experimental setup in Kalinin et al. (2010), we let

$$S_1(x) = 0.5x + 130 \quad \text{and} \quad S_2(x) = -0.03x + 20 \tag{19}$$

represent the concentrations of MeAsp and serine at each point $x \in [0, 400]$, respectively.

As we discussed in Sect. 3.2, since for any $\gamma > 0$,

$$V(x, \gamma) = \frac{\gamma}{1 + \gamma} \frac{0.5}{0.5x + 130} + \frac{1}{1 + \gamma} \frac{-0.03}{-0.03x + 20} \tag{20}$$

is decreasing on $[0, 400]$, $V(200, \gamma)$ is an increasing function of γ , and $V(200, \gamma^*) = 0$ for $\gamma^* \approx 0.985$, by Lemma 1, for $\gamma > 0.985$ (respectively, $\gamma < 0.985$) the bacteria move to the right (respectively, left), toward the gradient of MeAsp (respectively, serine).

Remark 3 In this example, for any $x \in [0, L]$, $S_1 > S_2$, $|S'_1| > |S'_2|$ and $|S'_1/S_1| > |S'_2/S_2|$. Therefore, one may expect that the bacterial always choose to move toward MeAsp (S_1). However, as we proved in Lemma 1, when the ratio Tar/Tsr is small enough ($\gamma < \gamma^*$), the bacteria move toward the gradient of serine. Figure 2 displays the relation between γ and the initial position of the bacteria, x_0 . The dotted curve $\gamma^*(x_0) = \left(\frac{S'_2/S_2}{S'_1/S_1}\right)(x_0) = \frac{780+3x_0}{2000-3x_0}$ satisfying $V(x_0, \gamma^*) = 0$ represents the bifurcation values in which the bacterial direction changes. As it is shown in Fig. 2, γ^* is an increasing function in x_0 , that is, $|S'_1/S_1|$ increases faster than $|S'_2/S_2|$ as x_0 increases. This means that if the bacteria start from near the right end point, a stronger force (a

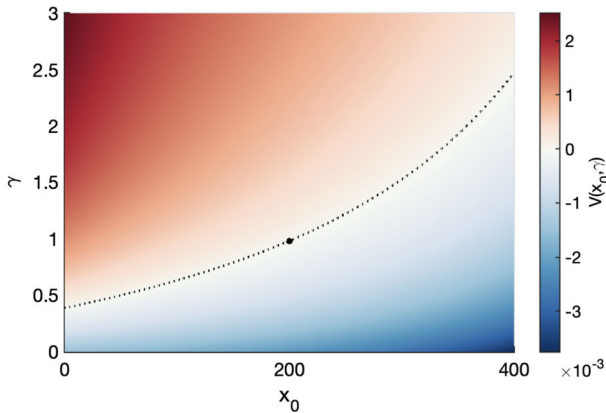


Fig. 2 Change of signs of V in (20) as x_0 and γ vary. For (x_0, γ) in the dark red (respectively, blue) region, V becomes positive (respectively, negative) as shown in the color bar. The dotted curve is a set of (x_0, γ^*) where $V = 0$. The solid point at $(200, 0.985)$ indicates the bifurcation value for the simulation in Sect. 3.3.1

larger γ^*) is needed to drag them toward the gradient of serine (S_2). In the following section with exponential gradients, although $S_1 > S_2$ and $S'_1 > S'_2$ everywhere, the needed force γ^* to drag the bacteria to the gradient of serine is always equal to 1. The reason is that $|S'_1/S_1| \equiv |S'_2/S_2|$, in that case.

To examine the result of Lemma 1, we choose two values for γ , $\gamma = 1.5 > \gamma^* \approx 0.985$ and $\gamma = 0.5 < \gamma^* \approx 0.985$, and Figure 3a, c displays distributions of the normalized density of *E. coli* obtained from the Monte Carlo agent-based simulation and numerical solution of the advection–diffusion (12). Three snapshots at times $t = 10, 60, 200$ (sec) are shown. As expected, the snapshots of a solution of (12) and the snapshots of a solution of Monte Carlo simulation move to the right when $\gamma > \gamma^*$, as shown in Fig. 3c, and they move to the left when $\gamma < \gamma^*$, as shown in Figure 3a.

Figure 3b, d displays the corresponding CMC_x which, as expected, is positive when $\gamma > \gamma^*$ and the bacteria accumulate on the right and are negative when $\gamma < \gamma^*$ and the bacteria accumulate on the left.

In Fig. 3, the adaptation speed rate p is 0.4 and other parameters are as given in Table 1. For the given linear stimuli, the values of γ and p are chosen such that the shallow condition (11) holds. Therefore, by Proposition 1, the advection–diffusion equation (12) approximates the Fokker–Planck equations (8)–(9). A comparison between numerical solutions of (12) and the solutions of Monte Carlo simulations in Fig. 3 confirms this result.

3.3.2 Chemotaxis in Response to Two Exponential Gradients

We now repeat the discussion of Section 3.3.1 for two opposing exponential gradients MeAsp and serine. We let

$$S_1(x) = 130e^{0.0023x} \quad \text{and} \quad S_2(x) = 8e^{-0.0023(x-400)} \tag{21}$$

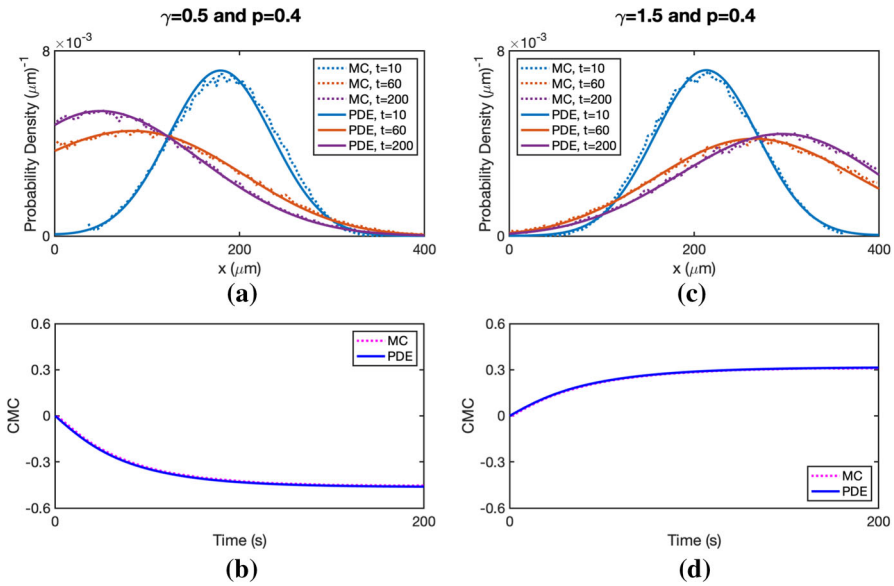


Fig. 3 a and c: Comparisons of Monte Carlo simulation and numerical solutions of (12) for two linear gradients (19) at times $t = 10, 60, 200$ (sec) with $\gamma = 0.5 < \gamma^*$ and $\gamma = 1.5 > \gamma^*$, in which the snapshots move to the left and right, respectively. b and (d): Comparisons of the corresponding CMC_x

represent the concentrations of MeAsp and serine at $x \in [0, 400]$, respectively. Exponential gradients have been used for various chemotaxis environments (e.g., Kalinin et al. (2009)). Here, $V(x, \gamma) = 0.0023 \frac{\gamma-1}{\gamma+1}$. By Lemma 1, the bifurcation value γ^* becomes 1, which is confirmed by choosing two values of $\gamma = 0.9$ and 1.1 , see Fig. 4.

Note that for the given exponential stimuli, the values of γ and $p = 0.05$ are chosen such that the shallow condition (11) holds. As discussed in Sect. 3.3.1, Proposition 1 and Figure 4 confirm that the numerical solutions of (12) agree well with the solutions of Monte Carlo simulations.

4 E. coli Preferences in Response to Two Stimuli in a Two-dimensional Space

In this section, we study the behavior of bacteria in response to two stimuli in a two-dimensional space. First, we derive the corresponding macroscopic equation; then analyze its steady-state behavior and discuss bacteria preferences. Then, we compare the numerical solutions of the model and Monte Carlo simulations and discuss how they agree with experimental results.

4.1 Advection–diffusion Equations and Integration of the Biochemistry of E. coli Chemotaxis

In this section, we assume that the bacteria move in a two-dimensional space. In a similar way to deriving the macroscopic equation (10) for a one-dimensional space,

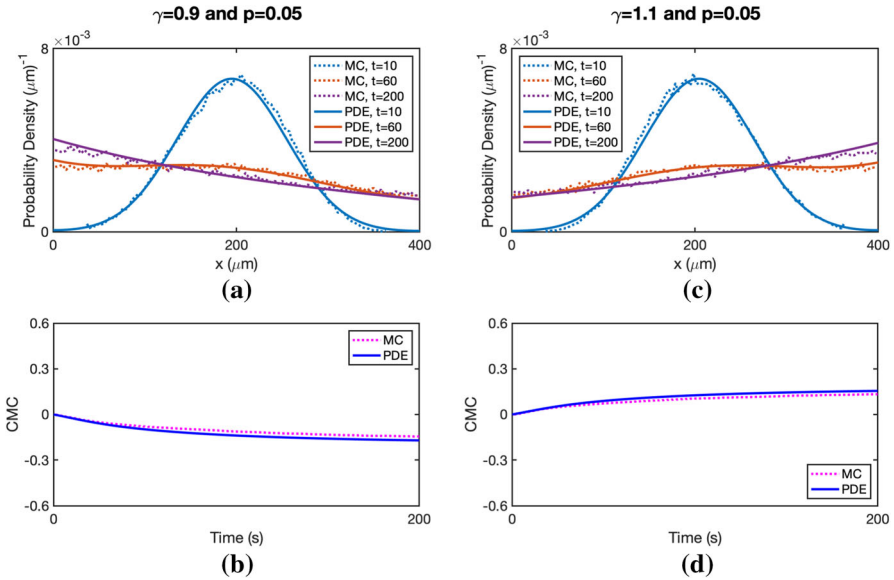


Fig. 4 **a** and **c**): Comparisons of Monte Carlo simulation and numerical solutions of (12) for two exponential gradients (21) at times $t = 10, 60, 200$ (sec) with $\gamma = 0.9 < \gamma^*$ and $\gamma = 1.1 > \gamma^*$, in which the snapshots move to the left and right, respectively. **b** and **d**: Comparisons of the corresponding CMC_x

an equation for the density of cells carrying the description of an internal state of individuals can be derived.

Let $p(\mathbf{x}, a, v, \theta, t)$ be a density function that describes a population of agents at time t and location $\mathbf{x} = (x, y)^\top$ with velocity $(v_1, v_2) = (v \cos \theta, v \sin \theta)$ and an internal state a . For the sake of simplicity, by fixing a constant speed v , we let $p_\theta(x, y, a, t)$ denotes the density of bacteria centered at $(x, y)^\top$ which move to the direction $(\cos(\theta), \sin(\theta))^\top$, $\theta \in [0, 2\pi)$, with the speed $v > 0$.

According to the forward Fokker–Planck equation (7), for $\theta \in [0, 2\pi)$, $p_\theta(x, y, a, t)$ satisfies

$$\begin{aligned} \frac{\partial p_\theta}{\partial t} + \frac{\partial}{\partial x} (v \cos(\theta) p_\theta) + \frac{\partial}{\partial y} (v \sin(\theta) p_\theta) + \frac{\partial}{\partial a} (f_\theta(a, S_1, S_2) p_\theta) \\ = \frac{1}{2\pi} \lambda(a, S_1, S_2) \int_0^{2\pi} (p_\eta(x, y, a, t) - p_\theta(x, y, a, t)) d\eta, \end{aligned} \tag{22}$$

where f_θ and λ describe the internal dynamics and tumbling rate, respectively.

In the presence of two extracellular signals $S_1(x, y, t)$ and $S_2(x, y, t)$, the evolution (6) of the internal state of the bacteria that move to the direction $(\cos(\theta), \sin(\theta))^\top$ with the speed v is governed by the following ordinary differential equation.

$$\begin{aligned} \frac{da}{dt} &= f_\theta(a, S_1, S_2) \\ &= f_0(a, S_1, S_2) + v \cos(\theta) f_1^1(a, S_1, S_2) + v \sin(\theta) f_1^2(a, S_1, S_2), \end{aligned} \tag{23}$$

where the real-valued functions f_θ, f_0, f_1^1 , and f_1^2 are continuously differentiable. We assume that f_0, f_1^1 and f_1^2 have the Taylor expansions with respect to a as follows:

$$f_0 = A_0 + A_1a + A_2a^2 + \dots, \\ f_1^i = B_0^i + B_1^i a + B_2^i a^2 + \dots, \quad i = 1, 2.$$

Also, we assume that the tumbling rate $\lambda = \lambda(a, S_1, S_2)$ has the Taylor expansion

$$\lambda = \alpha_0 + \alpha_1 a + \alpha_2 a^2 + \dots.$$

All the Taylor constants are functions of S_1 and S_2 .

At a fixed time t , consider a population of bacteria with internal dynamics (23) and tumbling rate λ that are located in (x, y) . The density of bacteria, described by

$$n(x, y, t) = \int_{\mathbb{R}} \int_0^{2\pi} p_\theta(x, y, a, t) d\theta da,$$

can be approximated by solving the following advection–diffusion equation:

$$\frac{\partial n}{\partial t} = \frac{1}{2} \frac{\partial}{\partial x} \left(\frac{v^2}{\alpha_0} \frac{\partial n}{\partial x} - \frac{v^2 \alpha_1 B_0^1}{\alpha_0(A_1 - \alpha_0)} n \right) + \frac{1}{2} \frac{\partial}{\partial y} \left(\frac{v^2}{\alpha_0} \frac{\partial n}{\partial y} - \frac{v^2 \alpha_1 B_0^2}{\alpha_0(A_1 - \alpha_0)} n \right). \tag{24}$$

The above equation is derived by applying moment closure techniques and parabolic scaling (Erban and Othmer 2004, 2005; Xue and Othmer 2009), (Aminzare and Sontag 2013; Xue 2015), and we provided a detailed derivation in Park and Aminzare (2020).

In accordance with the experimental setup of Kalinin et al. (2010) in which $L_1 \ll L_2$ and the population of bacteria is conserved in time, we impose zero flux boundary conditions along the boundary as follows:

For the spatial domain $[0, L_1] \times [0, L_2]$,

$$\begin{cases} D \frac{\partial n}{\partial x}(0, y, t) = \chi_1(0, y)n(0, y, t) & \text{and} & D \frac{\partial n}{\partial x}(L_1, y, t) = \chi_1(L_1, y)n(L_1, y, t) \\ D \frac{\partial n}{\partial y}(x, 0, t) = \chi_2(x, 0)n(x, 0, t) & \text{and} & D \frac{\partial n}{\partial y}(x, L_2, t) = \chi_2(x, L_2)n(x, L_2, t) \end{cases} \tag{25}$$

for any $t \geq 0$, where $D = \frac{v^2}{2\alpha_0}$ and for $i = 1, 2, \chi_i(x, y) = \frac{v^2 \alpha_1 B_0^i}{2\alpha_0(A_1 - \alpha_0)}$.

We now compute the coefficients of the macroscopic equation (24) for *E. coli* bacteria. As we discussed in Sect. 2.1, in a two-dimensional space, the internal state of *E. coli* evolves according to the following ODE:

$$\frac{da}{dt} = f_0(a, S_1, S_2) + v \cos(\theta) f_1^1(a, S_1, S_2) + v \sin(\theta) f_1^2(a, S_1, S_2),$$

where

$$\begin{aligned}
 f_0(a, S_1, S_2) &= \frac{\alpha}{\tau_a} Na(a - a_0)(a - 1), \\
 f_1^1(a, S_1, S_2) &= Na(a - 1) \left(\frac{\gamma}{1 + \gamma} \frac{\partial_x S_1}{S_1} + \frac{1}{1 + \gamma} \frac{\partial_x S_2}{S_2} \right), \\
 f_1^2(a, S_1, S_2) &= Na(a - 1) \left(\frac{\gamma}{1 + \gamma} \frac{\partial_y S_1}{S_1} + \frac{1}{1 + \gamma} \frac{\partial_y S_2}{S_2} \right).
 \end{aligned}$$

Note that the constant terms of the Taylor expansions of f_1^1 and f_1^2 are zero. These zero constant terms, in fact, cause a technical difficulty in deriving unique equation (24) when using the moment closure techniques, as we discussed in Park and Aminzare (2020). To fix this issue, we make a change of coordinate, $\hat{a} = a - a_0$, and obtain the following new internal dynamics of \hat{a} :

$$\frac{d\hat{a}}{dt} = \hat{f}_0(\hat{a}, S_1, S_2) + \nu \cos(\theta) \hat{f}_1^1(\hat{a}, S_1, S_2) + \nu \sin(\theta) \hat{f}_1^2(\hat{a}, S_1, S_2), \tag{26}$$

where

$$\begin{aligned}
 \hat{f}_0(\hat{a}, S_1, S_2) &= pN\hat{a}(\hat{a} + q)(\hat{a} + q - 1), \\
 \hat{f}_1^1(\hat{a}, S_1, S_2) &= N(\hat{a} + q)(\hat{a} + q - 1) \left(\frac{\gamma}{1 + \gamma} \frac{\partial_x S_1}{S_1} + \frac{1}{1 + \gamma} \frac{\partial_x S_2}{S_2} \right), \\
 \hat{f}_1^2(\hat{a}, S_1, S_2) &= N(\hat{a} + q)(\hat{a} + q - 1) \left(\frac{\gamma}{1 + \gamma} \frac{\partial_y S_1}{S_1} + \frac{1}{1 + \gamma} \frac{\partial_y S_2}{S_2} \right).
 \end{aligned}$$

We let

$$q = a_0 \quad \text{and} \quad p = \frac{\alpha}{\tau_a} \tag{27}$$

represent the adapted value and the speed of adaptation, respectively. We also transform the tumbling rate, discussed in (5), into the new coordinate \hat{a} as follows:

$$\lambda(\hat{a}) = \lambda_0 + r(\hat{a} + q)^H, \quad \text{where} \quad r = \frac{1}{\tau a_0^H}. \tag{28}$$

All the model parameters $N, p, q, r,$ and H are assumed to be positive constants and are as given in Table 1. Then, simple calculation show that the Taylor coefficients of $\hat{f}_0, \hat{f}_1^1,$ and \hat{f}_1^2 are

$$\begin{aligned}
 A_0 = 0, \quad A_1 = Npq(q - 1), \quad B_0^1 = Nq(q - 1) \left(\frac{\gamma}{1 + \gamma} \frac{\partial_x S_1}{S_1} + \frac{1}{1 + \gamma} \frac{\partial_x S_2}{S_2} \right), \\
 B_0^2 = Nq(q - 1) \left(\frac{\gamma}{1 + \gamma} \frac{\partial_y S_1}{S_1} + \frac{1}{1 + \gamma} \frac{\partial_y S_2}{S_2} \right), \quad \alpha_0 = \lambda_0 + rq^H, \quad \alpha_1 = \frac{rHq^H}{q}.
 \end{aligned}$$

We finally derive an advection–diffusion equation for *E. coli* chemotaxis, see Park and Aminzare (2020) for details.

Proposition 2 For any $\theta \in [0, 2\pi)$, the density functions p_θ satisfy the decay condition

$$p^\theta(x, y, a, t) \leq C(x, y, t)e^{-c(x,y,t)a}$$

for some functions $C, c : \mathbb{R}^2 \times [0, \infty) \rightarrow \mathbb{R}_{>0}$, and the stimuli S_1 and S_2 satisfy the shallow condition

$$\left| \cos(\theta) \left(\frac{\gamma}{1+\gamma} \frac{\partial_x S_1}{S_1} + \frac{1}{1+\gamma} \frac{\partial_x S_2}{S_2} \right) + \sin(\theta) \left(\frac{1}{1+\gamma} \frac{\partial_y S_1}{S_1} + \frac{1}{1+\gamma} \frac{\partial_y S_2}{S_2} \right) \right| \leq \frac{cp}{v} \tag{29}$$

for any $(x, y) \in [0, L_1] \times [0, L_2]$. Then, for the given internal dynamics (26), the dynamics of a population of *E. coli*, $n(x, y, t)$,

$$\frac{\partial n}{\partial t} = \nabla \cdot \left(D \nabla n - \chi \left(\frac{\gamma}{1+\gamma} \frac{\nabla_x S_1}{S_1} + \frac{1}{1+\gamma} \frac{\nabla_x S_2}{S_2} \right) n \right), \tag{30}$$

where the diffusion coefficient D and the advection constant χ are

$$D = \frac{v^2}{2(\lambda_0 + rq^H)} > 0, \quad \chi = \frac{rNHq^H(q-1)v^2}{2(\lambda_0 + rq^H)(Npq(q-1) - \lambda_0 - rq^H)} > 0.$$

For the spatial domain $[0, L_1] \times [0, L_2]$, the boundary conditions (25) become

$$\begin{cases} D \frac{\partial n}{\partial x}(0, y, t) = \chi V_1(0, y)n(0, y, t) & \text{and} & D \frac{\partial n}{\partial x}(L_1, y, t) = \chi V_1(L_1, y)n(L_1, y, t), \\ D \frac{\partial n}{\partial y}(x, 0, t) = \chi V_2(x, 0)n(x, 0, t) & \text{and} & D \frac{\partial n}{\partial y}(x, L_2, t) = \chi V_2(x, L_2)n(x, L_2, t), \end{cases} \tag{31}$$

where

$$V_1(x, y) = \frac{\gamma}{1+\gamma} \frac{\partial_x S_1}{S_1} + \frac{1}{1+\gamma} \frac{\partial_x S_2}{S_2} \quad \text{and} \quad V_2(x, y) = \frac{\gamma}{1+\gamma} \frac{\partial_y S_1}{S_1} + \frac{1}{1+\gamma} \frac{\partial_y S_2}{S_2}.$$

4.2 Bifurcation of Bacterial Chemotactic Preference

In a similar way to explaining the direction of bacterial migration in Section 3.2 through the bifurcation parameter γ , we explore properties of a steady-state solution of the advection–diffusion equation (30) and (31) and predict the direction of bacteria. To do this, we choose S_1, S_2 and γ so that continuous functions V_1 and V_2 on $[0, L_1] \times [0, L_2]$ satisfy

$$V_1(x, y) = V_1(x) \quad \text{and} \quad V_2(x, y) = V_2(y). \tag{32}$$

It is a sufficient condition to guarantee a unique non-trivial steady state of (30) and (31) when the initial condition $n(x, y, 0)$ is non-trivial, see Park and Aminzare (2020) for more details.

To compute the steady-state solution of the advection–diffusion equation (30) with zero flux boundary conditions (31), we let the flux at x direction and the flux at y direction be zero, i.e.,

$$\begin{aligned}
 J_x(x, y) &:= D \frac{\partial n}{\partial x} - \chi V_1(x, y)n = 0, \\
 J_y(x, y) &:= D \frac{\partial n}{\partial y} - \chi V_2(x, y)n = 0,
 \end{aligned}$$

which yield

$$\left(\frac{\partial}{\partial x} \log n \right) = \frac{\chi}{D} \left(\frac{V_1(x, y)}{V_2(x, y)} \right). \tag{33}$$

Note that this equation cannot be satisfied for any arbitrary V_1 and V_2 . Since the LHS is a gradient, a necessary and sufficient condition for the equation to hold is

$$\frac{\partial V_1}{\partial y} = \frac{\partial V_2}{\partial x}. \tag{34}$$

Note that (32) automatically satisfies (34). Under this condition, the steady-state solution can be obtained by simple integration of (33):

$$\Phi(x, y) = \Phi(c_1, c_2) \exp \left\{ \frac{\chi}{D} \left(\int_{c_1}^x V_1(z, y) dz + \int_{c_2}^y V_2(c_1, z) dz \right) \right\}, \tag{35}$$

where $(c_1, c_2) \in [0, L_1] \times [0, L_2]$ are chosen such that $\Phi(c_1, c_2)$ is a positive constant. Similar to what we discussed in Sect. 3.2, if $\partial V_1/\partial x \leq 0$ and $\partial V_2/\partial y \leq 0$, then the signs of V_1 and V_2 at the initial point (x_0, y_0) can determine the direction of the motion of bacteria. We let γ_1^* be the bifurcation value that determines the right/left direction (i.e., $V_1(x_0, y_0, \gamma_1^*) = 0$) and γ_2^* be the bifurcation value that determines the up/down direction (i.e., $V_2(x_0, y_0, \gamma_2^*) = 0$). Then, three scenarios are possible: (i) for $\max\{\gamma_1^*, \gamma_2^*\} < \gamma$, the bacteria move to the northeast and accumulate in $A_1 := \{x_0 < x < L_1, y_0 < y < L_2\}$; (ii) for $\min\{\gamma_1^*, \gamma_2^*\} < \gamma < \max\{\gamma_1^*, \gamma_2^*\}$ the bacteria either move to the southeast and accumulate in $A_4 := \{x_0 < x < L_1, 0 < y < y_0\}$ or move to the northwest and accumulate in $A_2 := \{0 < x < x_0, y_0 < y < L_2\}$; (iii) for $\gamma < \min\{\gamma_1^*, \gamma_2^*\}$, the bacteria move to the southwest and accumulate in $A_3 := \{0 < x < x_0, 0 < y < y_0\}$.

In the following section, we consider three sets of stimuli, which their corresponding V_1 and V_2 satisfy condition (32) (and hence (34)). For each set, we find the bifurcation values which determine the direction of bacteria.

4.3 Monte Carlo Agent-based Simulations in Two-dimensional Space

To validate the two-dimensional macroscopic approximation (30), we run a Monte Carlo simulation for microscopic equation (22). Our numerical experimental setup is very similar to that of Section 3.3, which we generalize to a two-dimensional space as follows. Note that since this work is motivated by Kalinin et al. (2010), we choose a computational setting to be qualitatively similar to the experimental setup of Kalinin et al. (2010) as well.

Spatial Domain. A channel of area of $400\mu\text{m}$ by $1600\mu\text{m}$ ($x \in [0, 400]$, $y \in [0, 1600]$).

Stimuli. Along the two sides of the channel $x = 0$ and $x = 400$, two opposing chemical signals $S_1(x, y)$ and $S_2(x, y)$, which, respectively, represent the concentrations of MeAsp and serine at (x, y) , flow and diffuse across the channel. Three sets of stimuli will be considered in Sects. 4.3.1–4.3.3.

Initial Condition. At $t = 0$ (sec), an ensemble of 100,000 agents is located in the center of the channel ($x = 200$ and $y = 800$).

Boundary Condition. We use reflecting boundary conditions at $x = 0, 400$ and $y = 0, 1600$ so the cells stay in the domain for all time.

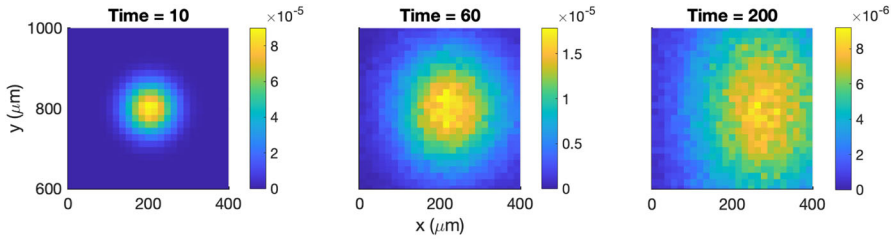
Simulation Duration. We simulate the bacterial behavior for $t \in [0, 200]$. In Sections 4.3.1 and 4.3.2, we observed that the solutions of the Monte Carlo simulation and the numerical solutions of (30) become stationary at $t = 200$.

The distributions of the solutions are displayed by using histograms with 2500 equal-sized bins. To solve the advection–diffusion equation (30) with boundary conditions (31), we use an explicit finite difference method. The summary of input data is given in Table 2. In what follows, we show some numerical results for three different choices of the stimuli combinations: Linear–Linear in Sect. 4.3.1, Exponential–Exponential in Sect. 4.3.2, and Linear \times Exponential–Linear \times Exponential in Sect. 4.3.3. We will show that (i) for some γ^* , when $\gamma > \gamma^*$, the bacteria move to the gradient of increasing MeAsp and when $\gamma < \gamma^*$, the bacteria move to the gradient of increasing serine; and (ii) under the shallow condition (29), the Monte Carlo agent-based simulations and the numerical solutions of (30) agree well.

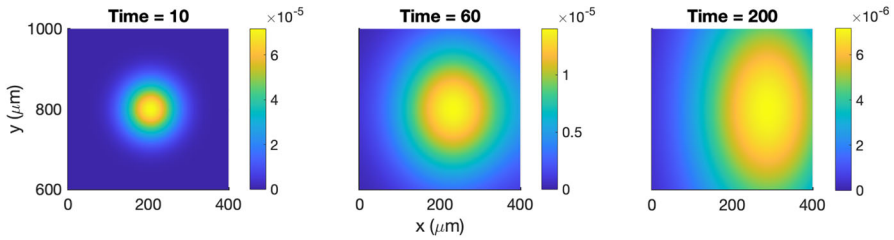
4.3.1 Chemotaxis in Response to Two Linear Gradients

Let $S_1(x, y) = 0.5x + 130$ and $S_2(x, y) = -0.03x + 20$ be two opposing linear gradients for MeAsp and serine, respectively. Note that the stimuli are constant with respect to y . In this case, $V_1(x, y) = V(x)$, as defined in Sect. 3.3.1, and $V_2(x, y) = 0$. Therefore, the condition (34) holds and the bacteria only move to the right or left (no up or down movement). Furthermore, the bifurcation value is equal to $\gamma^* \approx 0.985$, as computed in Sect. 3.3.1.

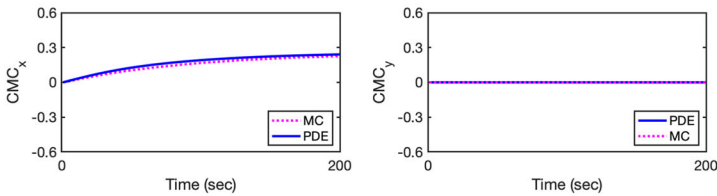
For the given linear gradients, Figure 5(a, b) (respectively, Figure 6(a, b)) displays the distributions of the normalized density of bacteria obtained from the Monte Carlo



(a) Monte-Carlo simulation for $\gamma = 1.5$ and $p = 1$



(b) Numerical solutions of (30) for $\gamma = 1.5$ and $p = 1$



(c) CMC_x (left) and CMC_y (right)

Fig. 5 a and b: Comparisons of the Monte Carlo simulations and numerical solutions of (30) in response to two linear gradients, when $\gamma = 1.5$. In this case the bacteria move to the right, the gradient of increasing MeAsp. c: Comparisons of the corresponding CMCs

agent-based simulation and numerical simulation of (30) for $\gamma = 1.5$ (respectively, $\gamma = 0.5$). The simulations are shown in three snapshots at times $t = 0$ (left), $t = 60$ (middle), and $t = 200$ (right). Figure 5c (respectively, Figure 6c) displays the corresponding CMCs in x -direction and y -direction.

In Figs. 5 and 6, the numerical solutions of (30) are in good agreement with the results of the agent-based simulation. The snapshots of the distribution move to the gradient of increasing MeAsp in Fig. 5 or serine in Fig. 6. Recalling the bifurcation value of $\gamma^* \approx 0.985$ in Sect. 3.3.1, these figures confirm that the chemotactic preference of bacteria depends on the relative abundances of receptors, i.e., when $\gamma = 1.1 > \gamma^*$, the bacteria move to the gradient of increasing MeAsp ($CMC_x > 0$ and increasing) and when $\gamma = 0.9 < \gamma^*$, the bacteria move to the gradient of increasing serine ($CMC_x < 0$ and decreasing). Note that these numerical examples qualitatively reproduce the bacterial behaviors observed in Kalinin et al. (2010).

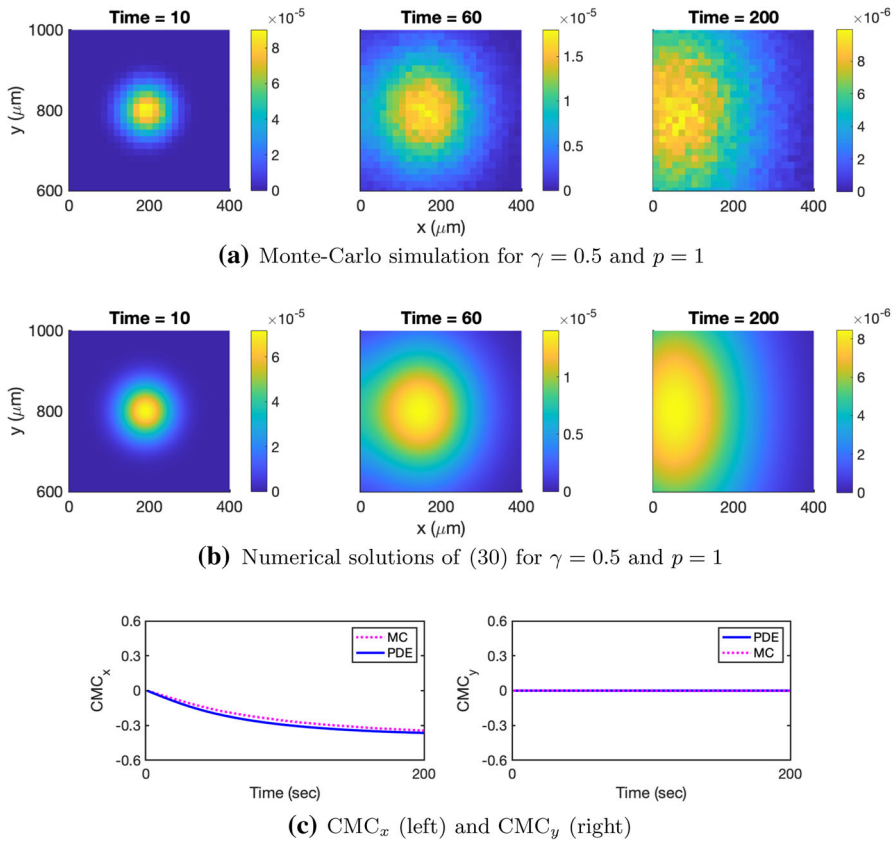


Fig. 6 **a** and **b**: Comparisons of the Monte Carlo simulations and numerical solutions of (30) for two linear gradients in (19), $\gamma = 0.5$, and $p = 1$. In this case, the bacteria move to the left, the gradient of increasing serine. Plots in (a) and (b) are displayed only for $(x, y) \in [0, 400] \times [600, 1000]$. (c): Comparisons of the corresponding CMCs

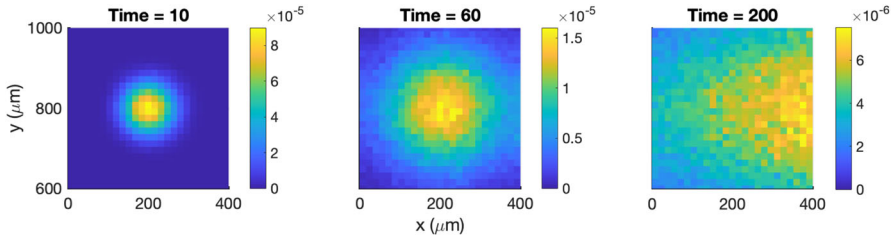
Since S_1 and S_2 are independent of y , the bacteria move in the y -direction very slightly, as evidenced by $CMC_y \approx 0$. Thus, although we run all the simulations on the domain $[0, 400] \times [0, 1600]$, we display a smaller domain, $[0, 400] \times [600, 1000]$.

4.3.2 Chemotaxis in Response to Two Exponential Gradients

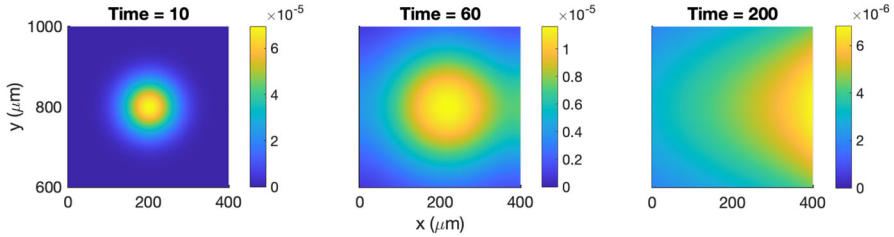
We assume that bacteria are exposed to two opposing exponential gradients

$$S_1(x, y) = 130e^{0.0023x} \quad \text{and} \quad S_2(x, y) = 8e^{-0.0023(x-400)}.$$

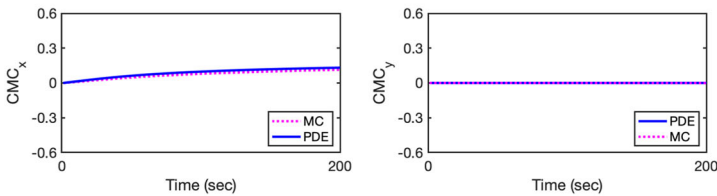
In this case, $V_1(x, y) = V(x)$, as defined in Sect. 3.3.2, and $V_2(x, y) = 0$. Therefore, condition (34) holds and the bacteria only move to the right or left (no up or down movement). Furthermore, the bifurcation value is equal to $\gamma^* = 1$, as computed in Sect. 3.3.2.



(a) Monte-Carlo simulation for $\gamma = 1.1$ and $p = 0.1$



(b) Numerical solutions of (30) for $\gamma = 1.1$ and $p = 0.1$



(c) CMC_x (left) and CMC_y (right)

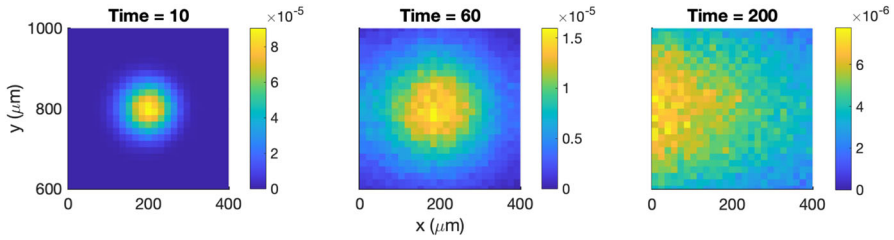
Fig. 7 a and b: Comparisons of Monte Carlo simulation and numerical solutions of (30) in response to two exponential gradients when $\gamma = 1.1$. Plots in (a) and (b) are displayed only for $(x, y) \in [0, 400] \times [600, 1000]$. (c): Comparisons of the corresponding CMCs

In Figs. 7 and 8, we compare the results of the Monte Carlo simulation with numerical solution of (30) and their corresponding CMCs. From the plots, we can see that (30) captures the behavior of individuals well. Recalling the bifurcation value $\gamma^* = 1$ of the ratio of Tar to Tsr in Sect. 3.3.2, as expected, the individuals travel to the right when $\gamma = 1.1 > \gamma^*$ as in Fig. 7 and move to the left when $\gamma = 0.9 < \gamma^*$ as in Fig. 8.

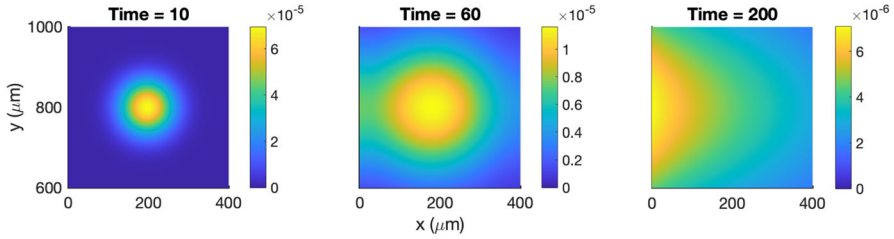
4.3.3 Chemotaxis in Response to Mixed Signals

In Sections 4.3.1 and 4.3.2, we used two opposing gradients, independent of y , to reproduce chemotaxis experiments in the literature. In what follows, we assume that two opposing gradients MeAsp (S_1) and serine (S_2) satisfy

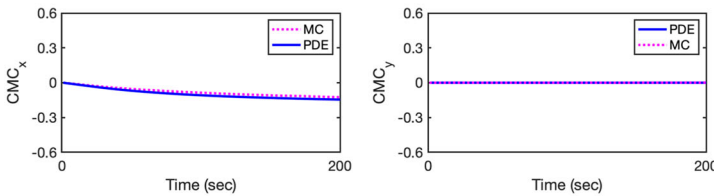
$$S_1(x, y) = (0.5x + 130)e^{0.005(y-800)} \quad \text{and} \quad S_2(x, y) = (-0.03x + 20)e^{-0.005(y-800)}. \tag{36}$$



(a) Monte-Carlo simulation for $\gamma = 0.9$ and $p = 0.1$



(b) Numerical solutions of (30) for $\gamma = 0.9$ and $p = 0.1$



(c) CMC_x (left) and CMC_y (right)

Fig. 8 a and b: Comparisons of Monte Carlo simulation and numerical solutions of (30) in response to two exponential gradients when $\gamma = 0.9$. Plots in a and b are displayed only for $(x, y) \in [0, 400] \times [600, 1000]$. c: Comparisons of the corresponding CMCs

Note that each gradient increases toward the corners $(0, 0)$ and $(400, 1600)$ on the boundary of the domain, and reaches a peak at the corners. In this case, $V_1(x, y) = V(x)$, as defined in Sect. 3.3.1, and $V_2(x, y) = 0.005 \frac{\gamma-1}{\gamma+1}$. Therefore, condition (34) holds. Furthermore, the bifurcation values are $\gamma_1^* \approx 0.985$, as computed in Sect. 3.3.1, and $\gamma_2^* = 1$. Therefore, three scenarios occur: (i) for $\gamma > 1$ the bacteria move to the northeast, (ii) for $0.985 < \gamma < 1$ the bacteria move to northwest, and (iii) for $\gamma < 0.985$ the bacteria move to southwest. As expected, the plots in Fig. 9 show that bacteria accumulate toward the corner $(400, 1600)$, when $\gamma = 1.5 > 1$. Also, the solution of (30) agrees well with the result of the Monte Carlo simulation.

5 Discussion

In this work, we studied the movement of a population of *E. coli* bacteria in response to two stimuli in a one- and a two-dimensional environment. Experimental results

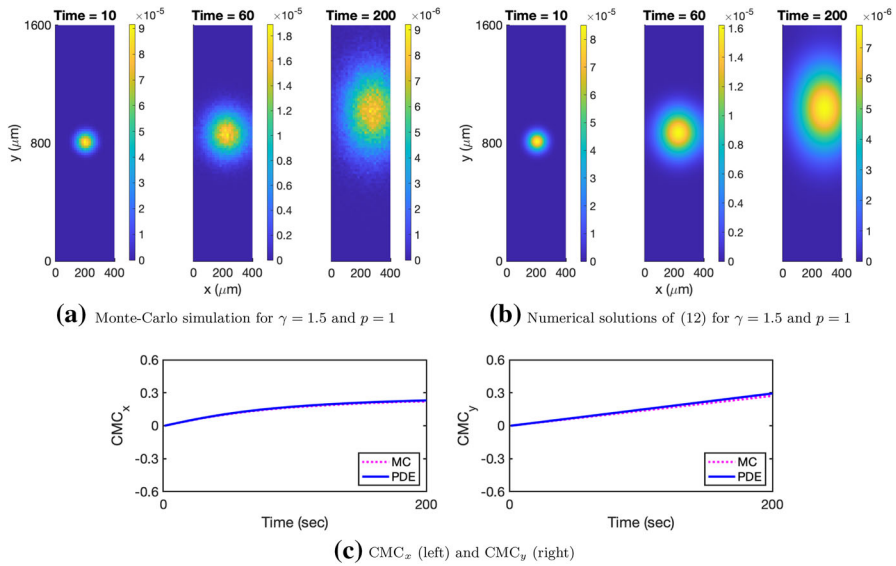


Fig. 9 a and b: Comparisons of Monte Carlo simulation and numerical solutions of (30) for gradients (36) for $\gamma = 1.5$. c: Comparisons of the corresponding CMCs

(Kalinin et al. 2010) show that the bacterial chemotactic preference to serine and MeAsp depends on the ratio of their chemoreceptors, namely $\gamma = \text{Tar}/\text{Tsr}$. In a shallow-gradient regime, we analytically found a threshold γ^* that determines the bacterial preference, i.e., if $\gamma > \gamma^*$, the bacteria move toward the gradient of MeAsp, and if $\gamma < \gamma^*$, the bacteria move toward the gradient of serine. We examined our results in an environment where one stimulus is dominant everywhere and observed that in such a situation, a bigger force γ^* might be needed to change the preference of the bacteria.

We started with a microscopic model for a population of bacteria carrying a one-dimensional internal dynamics. Indeed the microscopic equation is the forward Fokker–Planck equation of a stochastic model which describes bacterial chemotaxis (Stroock 1974). Then, we approximated the microscopic Fokker–Planck equation by a macroscopic advection–diffusion equation which is more tractable mathematically. We compared the numerical solution of the advection–diffusion equation with a Monte Carlo simulation of the bacterial chemotaxis to validate the approximation in a shallow-gradient regime.

The analysis in deriving the advection–diffusion equations is valid under the shallow-gradient condition. However, we numerically observed that even if the shallow-gradient condition does not hold, some of our results remain valid. For example, Figure 10 shows that under the condition of Section 3.3.1, the behavior of the bacteria does not change even when the adaptation rate p does not satisfy the shallow-gradient condition (gray region). We also observed that p does not affect the preference of bacteria. In fact, cells are often exposed to rapidly changing signals in vitro experiments and natural environments (see Xue (2015), Xue and Yang (2016) and references

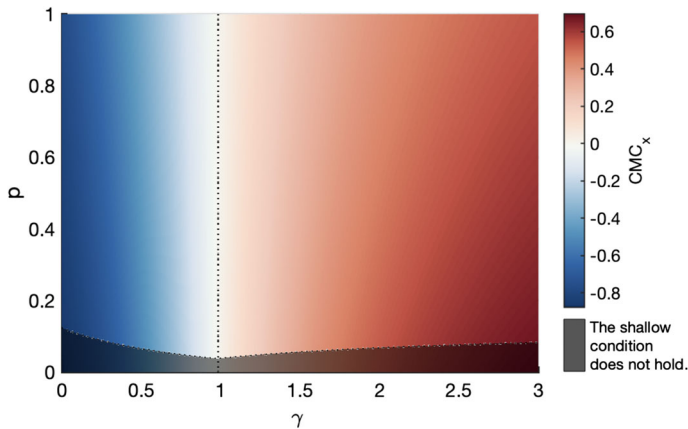


Fig. 10 How fast the signal changes or the adaptation speed does not affect the bacterial chemotactic preference. CMC_x of the steady state (17) for S_1 and S_2 in (19) for $x_0 = 200$. For (γ, p) in the dark red (respectively, blue) region, CMC_x becomes positive (respectively, negative) as shown in the color bar. For (γ, p) in the dark gray region, the shallow condition (11) is not satisfied. The dotted line represents $\gamma \approx 0.985$

therein), and great progress has been made in relaxing shallow gradient assumption Xue and Othmer (2009), Xue (2015), Xue and Yang (2016), Rousset and Samaey (2013), Gosztolai and Barahona (2020). Our work can be improved by considering a more general class of stimuli.

In Long et al. (2017), the authors found that *E. coli* cells respond to the gradient of chemoattractant not only by biasing their own random-walk swimming pattern through the intracellular pathway, but also by actively secreting a chemical signal into the extracellular medium, possibly through a communication signal transduction pathway. The extracellular signaling molecule is a strong chemoattractant that attracts distant cells to the food source. They showed that cell–cell communication enhances bacterial chemotaxis toward external attractants. Incorporating such chemoattractant into microscopic model is one of the main areas of our future investigation. This cell–cell communication can be modeled as an external force to each cell and described by an extra term into the LHS of (7), see Xue and Othmer (2009).

In this work, we only considered a one-dimensional internal dynamics. To obtain the internal dynamics of *E. coli* in response to multiple stimuli, we applied the heterogeneous MWC model (1) Hu and Tu (2014), Mello and Tu (2005), Keymer et al. (2006), which can capture the total activity level of bacterium affected by the stimuli and mathematically is tractable. In this global adaptation model, all receptors within the cluster are assumed to turn on and off simultaneously, and therefore, only the total kinase activity and total methylation level are considered. However, in a mixed-receptor cluster, it was found that receptor methylation dynamics is ligand specific and transient methylation crosstalk exists (Lan et al. 2011). Hence, a local adaptation model, such as Ising-type models (Lan et al. 2011; Keymer et al. 2006; Hu and Tu 2013), can better explain the adaptation dynamics of the mixed-receptor cluster. Such models require higher-dimensional equations to describe the internal dynamics. In our

future works, we generalize our result to two-dimensional internal dynamics and for each receptor Tar and Tsr, we will consider separate activity levels a_1 and a_2 instead of a in (1) and separate methylation dynamics dm_1/dt and dm_2/dt instead of (2), as described in Lan et al. (2011). Further, it would be great to consider the roles of the intratrimer and intertrimer interactions as the existing MWC-type or Ising-type model averages these interactions (Xin and Othmer 2012).

Acknowledgements The authors would like to thank Professor Eduardo Sontag for sharing the Matlab codes for one-dimensional space (used in Aminzare and Sontag (2013)) and Professor Hans Othmer for helpful discussions. This work is partially supported by the University of Iowa Old Gold Fellowship and Simons Foundation (712522) to ZA. The authors would also like to thank the anonymous referee who provided valuable suggestions and comments to improve this work.

Appendix

A brief description of Monte Carlo simulation: In a one-dimensional (respectively, two-dimensional) channel, we locate an ensemble of 100,000 agents in the center of the channel $x = 200$ (respectively, $(x, y) = (200, 800)$) at time $t = 0$. At each time step, the individuals choose a direction +1 or -1 (respectively, $(\cos(\theta), \sin(\theta))$, $\theta \in [0, 2\pi)$) at random, and move in that direction with a constant speed $v > 0$. At each time step, the internal dynamics of each individual are computed by Euler method. At the end of each time step, we choose a number between 0 and 1 randomly and compare the number with the probability of change from run to tumble in interval of length dt , namely $\lambda(a)dt$. If the turn occurs, the cell moves in the opposite direction with a probability of 0.5 (respectively, rotates by $\theta \in [0, 2\pi)$, where θ is chosen at random). If a cell is located outside the spatial domain, we relocate the cell by imposing reflecting boundary conditions.

See Tables 1 and 2.

Table 1 Parameters used in intracellular signaling pathway of *E. coli*

Equation	Parameter	Description	Value	References	
MWC model (1)	N	Number of receptors in a cluster, composed of Tar and Tsr	6	Jiang et al. (2010), Mello and Tu (2007)	
	r_1	Fraction of receptor Tar to MeAsp ^a			
	r_2	Fraction of receptor Tsr to serine ^{a†}			
	α	Free energy per added methylation group	1.7	Jiang et al. (2010), Sourjik and Berg (2002), Shimizu et al. (2006), Endres and Wingreen (2006)	
	m_0	Reference methylation level in the free energy	1	Jiang et al. (2010), Sourjik and Berg (2002), Shimizu et al. (2006), Endres and Wingreen (2006)	
	K_A^1	Dissociation constant of MeAsp to the active receptor Tar	18.2 μM	Kalinin et al. (2009), Jiang et al. (2010), Mello and Tu (2007), Lan et al. (2011)	
	K_A^2	Dissociation constant of serine to the active receptor Tsr	3 mM	Kalinin et al. (2009), Mello and Tu (2007), Lan et al. (2011)	
	K_I^1	Dissociation constant of MeAsp to the inactive receptor Tar	6 μM	Kalinin et al. (2009), Jiang et al. (2010), Lan et al. (2011)	
	K_I^2	Dissociation constant of serine to the active receptor Tsr	30 μM	Kalinin et al. (2009), Lan et al. (2011)	
	Adaptation model (2)	a_0	Adaptation level	0.5	Jiang et al. (2010), Berg and Tedesco (1975)
		τ_a	Adaptation time	Varies ^b	Vladimirov and Sourjik (2009)

Table 1 continued

Equation	Parameter	Description	Value	References
Run and tumble motion (5)	λ_0	Rotational diffusion	$0.28 \text{ rad}^2 \text{ s}^{-1}$	Sourjik and Berg (2002), Hu and Tu (2013)
	H	Hill coefficient of motor's response curve	10	Jiang et al. (2010), Sourjik and Berg (2002)
Transformed internal dynamics (27)	τ	Run average time	0.8 s	Jiang et al. (2010), Sourjik and Berg (2002)
	ν	Run velocity	$16.5 \mu\text{m s}^{-1}$	Jiang et al. (2010), Sourjik and Berg (2002)
	q	a_0	0.5	Kalinin et al. (2009)
	p	$\alpha\tau_a^{-1}$	Varies ^b	
Transformed tumbling rate (28)	γ	Ratio between Tar and Tsr receptors,	Varies ^a	
	r	$r_1 r_2^{-1}$		
		$(\tau a_0^H)^{-1}$	1280	Kalinin et al. (2009)

^a In this work, we are interested in the ratio of r_1 and r_2 satisfying $r_1 + r_2 = 1$. Instead of the range of r_1 and r_2 , we present the range of $\gamma = r_1/r_2$.
^b Bacterial adaptation time varies, and it depends on the strength of signals Vladimirov and Sourjik (2009). In this work, we vary p by choosing different τ_a between 1.7 and 34 as in Bray and Bourret (1995), Terwilliger et al. (1986), Simms et al. (1987)

Table 2 Input data used in numerical simulation

Expression	Value	Numerical partial differential equations ^a
	Monte Carlo simulation	
Spatial domain (\mathbf{x})	1D: $0 \leq x \leq 400(\mu m)$ 2D: $0 \leq x \leq 400(\mu m)$ and $0 \leq y \leq 1600(\mu m)$	
Time domain (t)	$0 \leq t \leq 200$ (sec) ^b	
Initial data	An ensemble of 100,000 agents poses in the center of each domain.	1D: $\exp\{-(x - 200)^2 / (2\varepsilon^2)\} / \sqrt{2\pi\varepsilon}$, $\varepsilon = 10^{-6}$ 2D: $\exp\{-(x - 200)^2 + (y - 800)^2 / (2\varepsilon^2)\} / 2\pi\varepsilon^2$, $\varepsilon = 10^{-6}$.
Boundary conditions	No flux boundary conditions	No flux boundary conditions: (16) for 1D and (31) for 2D
Spatial step size ($\Delta x, \Delta y$)	1D: $\Delta x = 0.01(\mu m)$ 2D: $\Delta x = \Delta y = 0.001(\mu m)$	1D: $\Delta x = 0.8(\mu m)^c$ 2D: $\Delta x = \Delta y = 0.8(\mu m)^c$
Time step size (Δt)	$\Delta t = 0.0001$ (sec) ^d	1D: $\Delta t = 0.0001$ (sec) 2D: $\Delta t = 0.0008$ for Sections 4.3.1, 4.3.2 and $\Delta t = 0.00025$ for Section 4.3.3 ^e
Ligand function (S_1, S_2)	· Dual linear gradients in Sections 3.3.1 and 4.3.1 : $S_1(x) = 0.5x + 130$ and $S_2(x) = -0.03x + 20$ · Dual exponential gradients in Sections 3.3.2 and 4.3.2 : $S_1(x) = 130e^{0.0023x}$ and $S_2(x) = 8e^{-0.0023(x-400)}$ · Mixed opposing gradients in Section 4.3.3 : $S_1(x, y) = (0.5x + 130)e^{0.005(y-800)}$ and $S_2(x, y) = (-0.03x + 20)e^{-0.005(y-800)}$	
Tar/Tsr ratio (γ) Adaptation ^e (p)	· Sections 3.3.1 and 4.3.1 : $\gamma = 1.5$ and $\gamma = 0.5$ with $p = 0.4$ (1D), 1 (2D). · Sections 3.3.2 and 4.3.2 : $\gamma = 1.1$ and $\gamma = 0.9$ with $p = 0.05$ (1D), 0.1 (2D) · Section 4.3.3 : $\gamma = 1.5$ and $p = 1$	

^a Finite difference method is used.

^b The solutions of the Monte Carlo simulation and advection–diffusion equations shown in Sections 3.3.1 to 4.3.2 become stationary at $t = 200$.

^c The time step size and the space step size in the finite difference formula satisfy Courant–Friedrichs–Lewy (CFL) condition and von Neumann stability analysis, respectively. It is confirmed that using smaller step sizes does not affect our results as long as the stability conditions are satisfied.

^d We choose small value for Δt to solve the dynamics of methylation by Euler method.

^e The values of p and γ satisfy the shallow condition.

References

- Alt W (1980) Biased random walk models for chemotaxis and related diffusion approximations. *J Math Biol* 9(2):147–177
- Aminzare, Z, Sontag ED (2013) Remarks on a population-level model of chemotaxis: advection-diffusion approximation and simulations. *arXiv preprint arXiv:1302.2605*
- Barkai N, Leibler S Robustness in simple biochemical networks. *Nature*, 387(6636):913–917
- Berg HC, Brown DA (1972) Chemotaxis in *Escherichia coli* analysed by three-dimensional tracking. *Nature* 239(5374):500–504
- Berg HC, Tedesco PM (1975) Transient response to chemotactic stimuli in *Escherichia coli*. *Proc Natl Acad Sci* 72(8):3235–3239
- Berg HC, Turner L (1990) Chemotaxis of bacteria in glass capillary arrays. *Escherichia coli*, motility, microchannel plate, and light scattering. *Biophys J* 58(4):919–930
- Bray D, Bourret RB (1995) Computer analysis of the binding reactions leading to a transmembrane receptor-linked multiprotein complex involved in bacterial chemotaxis. *Mol Biol Cell* 6(10):1367–1380
- Bren A, Welch M, Blat Y, Eisenbach M (1996) Signal termination in bacterial chemotaxis: CheZ mediates dephosphorylation of free rather than switch-bound CheY. *Proc Natl Acad Sci* 93(19):10090–10093
- Clausznitzer D, Oleksiuk O, Løvdok L, Sourjik V, Endres RG (2010) Chemotactic response and adaptation dynamics in *Escherichia coli*. *PLoS Comput Biol* 6(5):e1000784
- Demir M, Douarche C, Yoney A, Libchaber A, Salman H (2011) Effects of population density and chemical environment on the behavior of *Escherichia coli* in shallow temperature gradients. *Phys Biol* 8(6):63001
- Edgington MP, Tindall MJ (2018) Mathematical analysis of the *Escherichia coli* chemotaxis Signalling pathway. *Bull Math Biol* 80(4):758–787
- Endres RG, Wingreen NS (2006) Precise adaptation in bacterial chemotaxis through assistance neighborhoods. *Proc Natl Acad Sci* 103(35):13040–13044
- Endres RG, Oleksiuk O, Hansen CH, Meir Y, Sourjik V, Wingreen NS (2008) Variable sizes of *Escherichia coli* chemoreceptor signaling teams. *Mol Syst Biol* 4(1):211
- Erban R, Othmer HG (2004) From individual to collective behavior in bacterial chemotaxis. *SIAM J Appl Math* 65(2):361–391
- Erban R, Othmer HG (2005) From signal transduction to spatial pattern formation in *E. coli*: a paradigm for multiscale modeling in biology. *Multiscale Model. Simul.*, 3(2):362–394
- Gosztolai A, Barahona M (2020) Cellular memory enhances bacterial chemotactic navigation in rugged environments. *Commun Phys* 3(1):1–10
- Hansen CH, Sourjik V, Wingreen NS (2010) A dynamic-signaling-team model for chemotaxis receptors in *Escherichia coli*. *Proc Natl Acad Sci* 107(40):17170–17175
- Hu B, Tu Y (2013) Precision sensing by two opposing gradient sensors: how does *Escherichia coli* find its preferred pH level? *Biophys J* 105(1):276–285
- Hu B, Tu Y (2014) Behaviors and strategies of bacterial navigation in chemical and nonchemical gradients. *PLoS Comput Biol* 10(6):1003672
- Jiang L, Ouyang Q, Tu Y (2010) Quantitative modeling of *Escherichia coli* chemotactic motion in environments varying in space and time. *PLoS Comput Biol* 6(4):1000735
- Kalinin YV, Jiang L, Tu Y, Wu M (2009) Logarithmic sensing in *Escherichia coli* bacterial chemotaxis. *Biophys J* 96(6):2439–2448
- Kalinin Y, Neumann S, Sourjik V, Wu M (2010) Responses of *Escherichia coli* bacteria to two opposing chemoattractant gradients depend on the chemoreceptor ratio. *J Bacteriol* 192(7):1796–1800
- Keller EF, Segel LA (1971) Model for chemotaxis. *J Theor Biol* 30(2):225–234
- Keymer JE, Endres RG, Skoge M, Meir Y, Wingreen NS (2006) Chemosensing in *Escherichia coli*: two regimes of two-state receptors. *Proc Natl Acad Sci* 103(6):1786–1791
- Lai R-Z, Gosink KK, Parkinson JS (2017) Signaling consequences of structural lesions that alter the stability of chemoreceptor trimers of dimers. *J Mol Biol* 429(6):823–835
- Lan G, Schulmeister S, Sourjik V, Tu Y (2011) Adapt locally and act globally: strategy to maintain high chemoreceptor sensitivity in complex environments. *Molecular Syst Biol* 7(1):475
- Lazova MD, Ahmed T, Bellomo D, Stocker R, Shimizu TS (2011) Response rescaling in bacterial chemotaxis. *Proc Natl Acad Sci* 108(33):13870–13875
- Lipkow K (2006) Changing cellular location of CheZ predicted by molecular simulations. *PLoS Comput. Biol.* 2(4):39

- Lipkow K, Andrews SS, Bray D (2005) Simulated diffusion of phosphorylated CheY through the cytoplasm of *Escherichia coli*. *J Bacteriol* 187(1):45–53
- Long Z, Quaife B, Salman H, Oltvai ZN (2017) Cell-cell communication enhances bacterial chemotaxis toward external attractants. *Sci Rep* 7(1):1–12
- Macnab RM, Koshland DE (1972) The gradient-sensing mechanism in bacterial chemotaxis. *Proc Natl Acad Sci* 69(9):2509–2512
- Mello BA, Tu Y (2005) An allosteric model for heterogeneous receptor complexes: understanding bacterial chemotaxis responses to multiple stimuli. *Proc Natl Acad Sci* 102(48):17354–17359
- Mello BA, Tu Y (2007) Effects of adaptation in maintaining high sensitivity over a wide range of backgrounds for *Escherichia coli* chemotaxis. *Biophys J* 92(7):2329–2337
- Menolascina F, Rusconi R, Fernandez VI, Smriga S, Aminzare Z, Sontag ED, Stocker R (2017) Logarithmic sensing in *Bacillus subtilis* aerotaxis. *NPJ Syst Biol Appl* 3:16036
- Monod J, Wyman J, Changeux J-P (1965) On the nature of allosteric transitions: a plausible model. *J Mol Biol* 12(1):88–118
- Neumann S, Hansen CH, Wingreen NS, Sourjik V (2010) Differences in signalling by directly and indirectly binding ligands in bacterial chemotaxis. *The EMBO J* 29(20):3484–3495
- Othmer HG, Stevens A (1997) Aggregation, blowup and collapse: the ABCs of generalized taxis. *SIAM J Appl Math* 57(4):1044–1081
- Othmer HG, Dunbar SR, Alt W (1988) Models of dispersal in biological systems. *J Math Biol* 26:263–298
- Painter KJ, Maini PK, Othmer HG (2000) Development and applications of a model for cellular response to multiple chemotactic cues. *J Math Biol* 41(4):285–314
- Park J, Aminzare Z (2020) A Mathematical Description of Bacterial Chemotaxis in Response to Two Stimuli. arXiv preprint [arXiv:2006.00688](https://arxiv.org/abs/2006.00688)
- Rousset M, Samaey G (2013) Individual-based models for bacterial chemotaxis in the diffusion asymptotics. *Math Models Methods Appl Sci* 23(11):2005–2037
- Salman H, Libchaber A (2007) A concentration-dependent switch in the bacterial response to temperature. *Nat Cell Biol* 9(9):1098
- Shimizu TS, Delalez N, Pichler K, Berg HC (2006) Monitoring bacterial chemotaxis by using bioluminescence resonance energy transfer: absence of feedback from the flagellar motors. *Proc Natl Acad Sci* 103(7):2093–2097
- Shoval O, Goentoro L, Hart Y, Mayo A, Sontag E, Alon U (2010) Fold-change detection and scalar symmetry of sensory input fields. *Proc Natl Acad Sci* 107(36):15995–16000
- Shoval O, Alon U, Sontag E (2011) Symmetry invariance for adapting biological systems. *SIAM J Appl Math* 10(3):857–886
- Simms SA, Stock AM, Stock JB (1987) Purification and characterization of the s-adenosylmethionine: glutamyl methyltransferase that modifies membrane chemoreceptor proteins in bacteria. *J Biol Chem* 262(18):8537–8543
- Sourjik V, Berg HC (2002) Receptor sensitivity in bacterial chemotaxis. *Proc Natl Acad Sci* 99(1):123–127
- Spiro, P. A., Parkinson, J. S., Othmer, H. G.: A model of excitation and adaptation in bacterial chemotaxis. *Proc. Natl. Acad. Sci.*, 94(14):7263–7268
- Springer WR, Koshland DE (1977) Identification of a protein methyltransferase as the cheR gene product in the bacterial sensing system. *Proc Natl Acad Sci* 74(2):533–537
- Stock JB, Koshland DE (1978) A protein methyltransferase involved in bacterial sensing. *Proc Natl Acad Sci* 75(8):3659–3663
- Stroock DW (1974) Some stochastic processes which arise from a model of the motion of a bacterium. *Z Wahrscheinlichkeitstheor verw Geb* 28(4):305–315
- Terwilliger TC, Wang JY, Koshland DE (1986) Kinetics of receptor modification. The multiply methylated aspartate receptors involved in bacterial chemotaxis. *J Biol Chem* 261(23):10814–10820
- Tindall MJ, Maini PK, Porter SL, Armitage JP (2008) Overview of mathematical approaches used to model bacterial chemotaxis II: bacterial populations. *Bull Math Biol* 70(6):1570
- Tu Y, Shimizu TS, Berg HC (2008) Modeling the chemotactic response of *Escherichia coli* to time-varying stimuli. *Proc Natl Acad Sci* 105(39):14855–14860
- Vladimirov N, Sourjik V (2009) Chemotaxis: how bacteria use memory. *Biol Chem* 390(11):1097–1104
- Vladimirov N, Løvold L, Lebedz D, Sourjik V (2008) Dependence of bacterial chemotaxis on gradient shape and adaptation rate. *PLoS Comput. Biol* 4(12):e1000242
- Wadhams GH, Armitage JP (2004) Making sense of it all: bacterial chemotaxis. *Nat Rev Mol Cell Biol* 5(12):1024–1037

- Welch M, Oosawa K, Aizawa S-L, Eisenbach M (1993) Phosphorylation-dependent binding of a signal molecule to the flagellar switch of bacteria. *Proc Natl Acad Sci* 90(19):8787–8791
- Xin X, Othmer HG (2012) A trimer of dimer based model for the chemotactic signal transduction network in bacterial chemotaxis. *Bull Math Biol* 74(10):2339–2382
- Xue C (2015) Macroscopic equations for bacterial chemotaxis: integration of detailed biochemistry of cell signaling. *J Math Biol* 70(1):1–44
- Xue C, Othmer HG (2009) Multiscale models of taxis-driven patterning in bacterial populations. *SIAM J Appl Math* 70(1):133–167
- Xue C, Yang X (2016) Moment-flux models for bacterial chemotaxis in large signal gradients. *J Math Biol* 73(4):977–1000
- Yang Y, Sourjik V (2012) Opposite responses by different chemoreceptors set a tunable preference point in *Escherichia coli* pH taxis. *Molecular Microbiol* 86(6):1482–1489

Publisher's Note Springer Nature remains neutral with regard to jurisdictional claims in published maps and institutional affiliations.